DOI 10.1007/s11237-026-09862-2
*Theoretical and Experimental Chemistry, Vol. 61, No. 3, July, 2025 (Ukrainian Original Vol. 61, No. 3, May-June, 2025)*

# CHIRALITY IN BIOLOGY, LUMINESCENCE, CATALYSIS, AND SPINTRONICS: AN ANALYSIS OF NEW APPROACHES: A REVIEW

**T. V. Sakhno,[1] B. P. Minaev,[2] and Y. E. Sakhno[3]**

UDC 541.128+577.1+544.421.2+535.37+538.9

*Current hypotheses and experimental data concerning the origin of biological homochirality, a phenomenon in which living systems predominantly use L-amino acids and D-sugars, are analyzed in the review. Various physical and chemical factors that may lead to the formation of an enantiomeric excess are considered.*

***Keywords****: homochirality, chiral selection, CISS effect, autocatalysis, photochemistry, biochemical evolution, oxygen evolution reactions.*

## INTRODUCTION

Chirality is a geometric property of objects that cannot be superimposed on their mirror image, similar to the distinction between the right and left hands. In chemistry, this term refers to molecules that exist as enantiomers, in particular, pairs of structures that cannot be overlaid due to the spatial arrangement of their atoms. Most biologically essential molecules, such as amino acids and sugars, are chiral and occur in living systems predominantly in only one of the possible forms (e.g., L-amino acids or D-sugars). This phenomenon is known as homochirality. It is a defining feature of biological systems and, at the same time, one of the most significant unresolved mysteries concerning the origin of life on Earth [1]. The origin of biological homochirality is actively studied, particularly in the context of potential physical, chemical, and astrophysical mechanisms responsible for the initial breaking of chiral symmetry [2-5]. Chirality is of fundamental importance for biochemical processes, as even minor differences between enantiomers can profoundly influence their biological activity, reaction pathways, and molecular interactions. Furthermore, recent studies have demonstrated that chiral molecules can affect electron spin, one of the fundamental quantum properties of particles. This finding underpins the concept of chiral-induced spin selectivity (CISS), which opens new prospects in catalysis, photonics, and spintronics. The CISS phenomenon has attracted considerable interest both at the theoretical level and due to its practical implications.

This review aims to systematize current concepts on the origin and manifestations of chirality in natural and synthetic systems, as well as to analyze the key mechanisms underlying the formation of homochirality, particularly in the context of their relationship with functional materials, photocatalysis, and the CISS effect.

[1] Poltava State Agrarian University, Poltava, Ukraine. E-mail: sakhno2003@ukr.net.
[2] Bohdan Khmelnytskyi National University of Cherkasy, Cherkasy, Ukraine.
[3] University of Delaware, Newark, USA.

Translated from Teoretychna ta Eksperymentalna Khimiya, Vol. 61, No. 3, pp. 135-156, May-June, 2025. Received July 25, 2025; accepted September 15, 2025.

## BIOLOGICAL HOMOCHIRALITY

Biological homochirality is a unique phenomenon in which living organisms predominantly utilize only one enantiomer, such as L-amino acids in proteins or D-sugars in helices of DNA and RNA [6]. This phenomenon has been recognized since the mid-20th century, when a systematic chiral preference in biomolecules was discovered. The term *homochirality* was widely adopted in the works of Bonner (1970-1990) [7]. Early ideas on this subject can be traced back to Louis Pasteur (1848) and Calvin (1953) [7].

In chemistry, chirality is associated with the absence of a plane of symmetry in a molecule; such molecules possess enantiomers that differ in biological activity and in their interaction with circularly polarized light (CPL) [8, 9]. Hypotheses regarding the origin of homochirality on the early Earth include asymmetric photolysis induced by CPL, particularly from neutron stars [10], as well as the influence of the first organic acids delivered by meteorites. Chiral signatures have been detected in meteorite ice; during their prolonged journey through the galaxy, these molecules were likely exposed to CPL radiation from supernovae. Consequently, a chiral imbalance may have been present in prebiotic organic material, which was presumably utilized about three billion years ago in the emergence of life on Earth. Other hypotheses consider the role of spin-polarized electrons [11]. Protein homochirality determines the stereospecificity of enzymatic reactions [7]. It is also linked to the chirality of CPL sources: chiral luminophores emit light with circular polarization [12-15]. Chiral prismatic [4]arenes were synthesized for the first time in [16], suitable for molecular recognition with a high asymmetry factor ($g_{lum}$), which quantifies the degree of circular polarization of emission and is defined as the ratio of the difference in intensities of left- and right-circularly polarized light to their sum $g_{\mathrm{lum}}^{\max} = 2$. Review [17] addresses the "electric dipole revolution", novel approaches to controlling chiral states in light emission involving chiral luminophores.

Biochemical chirality itself determines selective pharmacological activity: "incorrect" enantiomers can be toxic, as in the case of thalidomide [18]. Thalidomide became a historical example of how neglecting chirality can lead to catastrophic consequences. Today, the development of all new chiral pharmaceuticals requires mandatory study of individual enantiomers [19]. A hypothesis was proposed in [20] that evolution began from a chirally neutral state, and the dominance of one form was the result of chance. The authors also suggest that alternative chirality might have existed on early Earth or other planets. It is demonstrated in [21] that crystallization can naturally generate initial chiral asymmetry, as the nucleation process, the first stage of crystal formation, is stochastic in nature. Therefore, a general and prebiotically plausible one-step mechanism was proposed for the transition from an ideally racemic solution to a homochiral suspension. This concept is supported by (1) theoretical arguments, (2) modeling using a first-principles mathematical model, and (3) experimental studies with the chiral compound N-(2-methylbenzylidene)-phenylglycinamide. Both modeling and experimental results confirm the proposed theory.

The formation of diastereomeric complexes between enantiomers and a chiral selector is the primary mechanism ensuring selectivity in chiral recognition processes. The difference in Gibbs free energy between these complexes determines their relative stability and, consequently, the interaction energy [22]. Historically, the chiral recognition model was proposed as a three-point (minimal) interaction model, according to which effective enantioselective interaction requires at least three points of contact between an asymmetric compound (enantiomer) and a chiral selector (e.g., an enzyme or receptor). Fig. 1a illustrates the ideal fit of one enantiomer to three interaction points on the selector, ensuring strong binding. Conversely, Fig. 1b shows that its mirror image, regardless of orientation, can form at most two effective contacts. This spatial difference underlies the selective binding of one enantiomer, which constitutes the essence of enantiorecognition. Importantly, all three interactions were considered attractive forces in the original model. However, according to modern stereochemical views, repulsive interactions are also regarded as significant. Thus, a single favorable interaction can enable the formation of a stable diastereomeric complex even with two contacts involving repulsion. Key conditions of the three-point model include: (1) the presence of three simultaneous interaction points and (2) the involvement of three distinct substituents attached to the stereochemical center. Two interaction points oriented toward the same substituent, while increasing overall binding energy, do not enhance enantioselectivity. This model has found practical application in enzymatic reactions, chromatographic separation of enantiomers, and molecular design of chiral receptors, explaining the mechanism of action in many natural and synthetic systems.

The effect of self-induced diastereomeric anisochronism (SIDA) was studied in 35 newly synthesized amine derivatives in [23], revealing structure-activity relationships as well as the role of hydrogen bonding and solvent effects. A

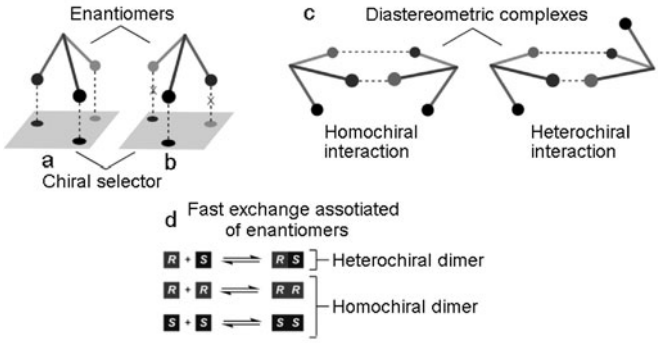


Fig. 1. Three-point interaction model. A chiral molecule with an asymmetric carbon atom may possess three substituent groups that can align precisely with three sites of the selector (a). Its mirror image, even after all possible rotations, can match at most two groups capable of interacting with only two selector sites (b). Consequently, the binding constant for the chiral molecule in example (a) will be higher than the corresponding constant for its mirror image. Self-recognition of enantiomers occurs through the formation of transient homo- and heterochiral associates (c). Origin of the SIDA effect (d). Adapted with permission from [22] © 2006 American Chemical Society.

generalized interaction profile method for functional groups was proposed to optimize the selection of the medium. SIDA represents an efficient tool for determining enantiomeric purity without the need for chromatography. Fig. 1 schematically illustrates the principal types of interactions underlying chiral recognition. A diastereomeric complex is formed through non-covalent interactions between chiral molecules sharing the same absolute configuration (e.g., R–R or S–S). Such homochiral interactions are generally more stable due to spatial complementarity and the matching of chiral surfaces. On the right, a heterochiral interaction between enantiomers of opposite configuration (e.g., R–S) is depicted. In this case, steric mismatch between substituents limits the number of effective contact points, reducing the stability of the complex compared to its homochiral counterpart. Complementary binding sites (indicated by dashed lines) refer to functional groups or local regions on the chiral selector that enable specific recognition and selective interaction with particular substituents of the chiral guest molecule.

## NATURAL CHIRAL AGENTS CAPABLE OF BREAKING SYMMETRY

Although enantiomers share the same chemical formula and topology, their three-dimensional structures differ, which determines enantioselective interactions with chirally sensitive agents. Among the potential factors responsible for natural disruption of chiral symmetry are: circularly polarized light, asymmetric β-decay, chiral minerals, magnetic fields (the CISS effect), cosmic radiolysis, and homochiral catalysts.

**Circularly Polarized Light (CPL)**. CPL can induce enantioselective photolysis, leading to an enantiomeric excess [14]. Under terrestrial conditions, CPL is not observed; however, its sources include cosmic objects such as stars, pulsars, active galactic nuclei, and nebulae. The most extensively studied example is the Orion Molecular Cloud (OMC-1), where infrared CPL has been detected [24, 25]. CPL is capable of promoting the formation of chiral organic molecules in interstellar clouds or in icy mantles of comets and meteorites. For instance, the Murchison meteorite exhibited an L-enantiomeric excess of amino acids [26], consistent with CPL influence in space. Cosmic в-radiation, particularly spin-polarized electrons emitted by isotopes such as $^{60}$Fe and $^{26}$Al, may also have contributed to asymmetric processes in the interstellar medium, thereby facilitating chiral perturbation [27].

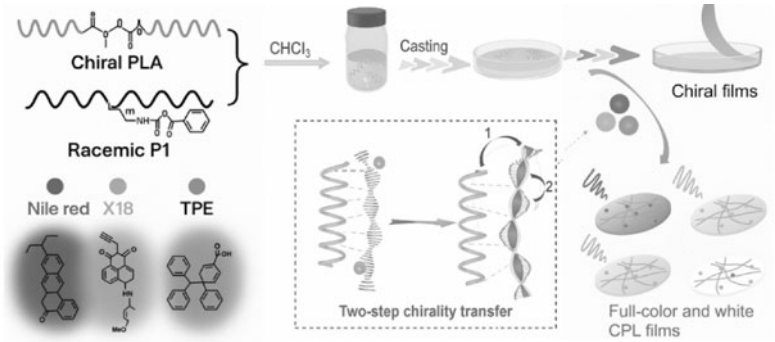


Fig. 2. Schematic representation of chirality transfer and CPL generation across the entire visible spectrum in polymer composite films. Reproduced from [18] with permission of © 2006 American Chemical Society.

**Laboratory Simulation**. Artificially generated CPL is employed to simulate cosmic conditions. Laboratory experiments have demonstrated that UV-CPL irradiation of interstellar ice analogs results in the formation of amino acids with a non-racemic excess of up to 1.34% for $^{13}$C-alanine [28, 29]. In another study, the asymmetric photolysis of racemic pyrimidyl alkanol under CPL, followed by autocatalytic amplification, resulted in compounds exhibiting an enantiomeric excess (*ee)* of > 99.5% [30]. These findings support the hypothesis that CPL could have acted as a primary chiral perturbation factor under prebiotic conditions.

**Photoelectron Circular Dichroism (PECD)**. PECD represents another potential mechanism for chiral selection that does not require an external chiral environment. It has been demonstrated that under Lyman-α irradiation, the enantiomeric excess of proline in the gas phase can reach up to 4% [31, 32]. A similar effect has also been observed for alanine [33].

**Photodesorption.** CPL can also induce enantioselective desorption from surfaces. For example, preferential desorption of one enantiomer was observed when BINOL films were irradiated with circularly polarized light [34], which is significant for enantiomer separation techniques.

**Chiral Transfer in Polymeric Systems.** The transfer of chirality within polymer composites is one of the innovative approaches to designing materials with controllable chiroptical properties. Specifically, chiral polylactide (PLA) can induce helical chirality in achiral polyacetylene (P1), which inherently lacks chiral features. This chirality transfer is accompanied by the emergence of circularly polarized luminescence (CPL) across a broad spectral range, including even white light, opening prospects for applications in optoelectronics, sensors, CPL-based displays, and quantum technologies. A two-stage mechanism of chiral transfer in solid composite films was reported in [18]. The mechanism involves: chirality transfer from PLA to polyacetylene P1. Biodegradable chiral PLA acts as both the source of chirality and the structural matrix of the film. Racemic polyacetylene P1 acquires a helical chiral structure in the presence of PLA. The primary driving force of this process is hydrogen bonding between PLA and P1 polymer chains, resulting in pronounced optical activity in an initially achiral polymer. Transfer of induced chirality to fluorophores: The second stage involves transferring the induced chirality from P1 to achiral fluorescent molecules embedded in the composite film. Consequently, CPL is generated across the entire visible spectrum from red to blue components of white light. This process is schematically illustrated in Fig. 2 [18].

This opens up promising opportunities for optoelectronics and sensors. The resulting CPL-active films demonstrated efficiency in the structure of prototype organic light-emitting diodes (CP-OLEDs), where selective emission of right or left CPL is achieved without external optical components. Therefore, the study presents a universal, straightforward, and scalable strategy for developing functional chiroptical materials capable of direct CPL generation with stable and controllable chirality.

**Astrochemical Aspects.** Certain molecules, such as oxirane and vinyloxirane, are considered potential chiral markers in space. The CHARISMA database has been proposed to facilitate the search for absorption bands of chiral molecules within the spectral range of 700 MHz to 25 GHz, which encompasses rotational transitions characteristic of small organic compounds and is a priority for astronomical identification of chiral molecules in the interstellar medium using next-generation telescopes [35]. The search for a second chiral molecule beyond propylene oxide remains an active area of astrochemical research.

**CPL Photodetectors.** The development of chiral materials for detecting CPL without external optical components represents a promising research direction. New sensitivity limits (up to 1340 nm) and enhanced performance have been established in chiral perovskites and metamaterials [36].

**Processes that Selectively Reduce the Concentration of One Enantiomer (Enantioselective Degradation)**

Although these processes do not generate new chirality, they can disrupt the racemic symmetry of a system by producing an enantiomeric excess (*ee*) through the selective destruction of one enantiomer. Examples of mechanisms responsible for such degradation are presented below.

**Circularly Polarized Light.** Left- or right-polarized UV radiation can be selectively absorbed by only one of the enantiomers (for example, the D-form), leading to its degradation and, consequently, to the accumulation of the other enantiomer (L). This phenomenon may result in a slight but directional enantiomeric excess (*ee*).

**Asymmetric β-Radiation from Atomic Nuclei**. Streams of beta electrons with a specific spin orientation can selectively interact with enantiomers, altering their stability or causing the selective degradation of one of them.

**Enantioselective Adsorption on Chiral Minerals.** A study published in Symmetry [4, 5] demonstrated that α-quartz can selectively adsorb one enantiomer of amino acids such as alanine and leucine. This finding supports the potential role of natural chiral minerals in the emergence of biological homochirality.

**Chiral Polymers as Substrates.** Polylactide (PLA) and other chiral polymers are employed as solid-phase carriers in studies on the effect of CPL on the enantioselective photolysis of amino acids. In one experiment, amino acids were deposited onto a chiral polymer supporter and irradiated with circularly polarized UV light, enabling the study of selective cleavage of isomers [18].

**Radiolysis/Photolysis on Chiral Substrates.** The interaction of ionizing radiation (e.g., γ-rays) or UV photons with chirally active surfaces can induce enantioselective cleavage of molecules. Such processes are considered promising for modeling conditions under which the initial chiral imbalance might have arisen in prebiotic systems.

Amino acids enriched in an L-enantiomer, such as isovaline, have been detected in CM-type meteorites, extraterrestrial carriers of organic molecules, suggesting a possible interstellar origin of chiral asymmetry [37]. In this study, racemic leucine was irradiated with ultraviolet circularly polarized radiation at the DESIRS beamline of a Soleil synchrotron. Photolysis of more than 99% of leucine was recorded. The highest induced enantiomeric excess (*ee*) of 5.2% for the D-leucine enantiomer was achieved under irradiation with r-CPL at 187 nm and a photolysis degree of 99.23% [37]. It was established that the L-enantiomer degrades more slowly under right-polarized CPL, indicating the possibility of selective photolysis.

One of the most compelling pieces of evidence for the involvement of abiotic processes in the emergence of chiral imbalance is the detection of significant enantiomeric enrichment of L-proteinogenic amino acids in the Tagish Lake meteorite [38]. Substantial excesses of L-enantiomers of aspartic and glutamic acids (up to 59%) were recorded in three different fragments of the C2-type carbonaceous chondrite, whereas alanine, another α-H-amino acid, remained nearly racemic. The isotopic signatures of amino acids differed markedly from terrestrial values, confirming their extraterrestrial origin. The authors attribute this to the peculiarities of conglomerate amino acid crystallization during aqueous alteration on the meteorite's parent body. Such processes likely amplified a minor initial chiral imbalance caused by ionization or UV radiation, ultimately leading to significant enantiomeric enrichment. These findings support the hypothesis that abiotic origins of chiral excess are possible in prebiotic systems through radiolysis, photolysis, and crystallization processes.

**Processes that Catalyze the Formation of a Single Enantiomer (Enantioselective Synthesis).** This group includes mechanisms capable of actively generating chiral molecules from achiral or weakly chiral precursors. One example is crystallization with chiral resolution, where a single chiral crystal forms from a racemic or achiral mixture. Such a process is considered a possible instance of spontaneous symmetry breaking. Thus, enantioselective degradation processes can reduce the concentration of one enantiomer, whereas catalysis promotes the selective formation or amplification of the other. It is likely that, during the early stages of Earth's chemical evolution (or under extraterrestrial conditions), these two mechanisms operated either in parallel or sequentially, facilitating the gradual transition toward biological homochirality.

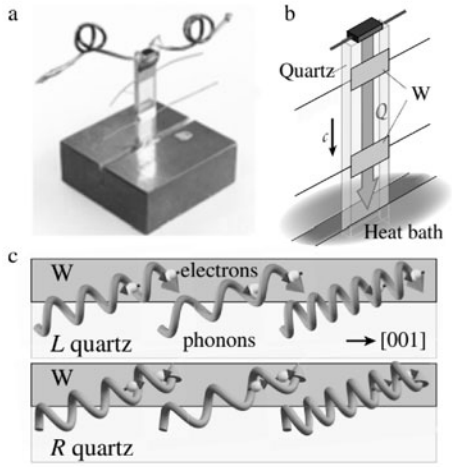


Fig. 3. Image (a) and scheme (b) of a device fabricated on a quartz supported with tungsten (W) electrodes. The copper thermal bath measures 10×10×4 mm and contains a groove 2 mm deep and 0.5 mm wide. The transverse voltage is defined between electrodes located on the upper and lower surfaces of the supporter. Scheme of the propagation and leakage of phonons interacting with electrons in an electrode on quartz (c). Adapted from [47].

**Dynamic Induction of Enantiomeric Excess**

Ribo et al. [39] demonstrated that mechanical stirring of solutions of achiral diprotonated porphyrins in the mesophase can induce not only spontaneous breaking of chiral symmetry but also controlled induction of chiral sign depending on the direction of the vortex. According to circular dichroism (CD) spectroscopy data, this represents an example of unstable bifurcation under nonequilibrium conditions, where external mechanical influence directs the process into a specific chiral channel. Another study [40] shows that chiral order can emerge in achiral nematic liquid crystals under flow in microfluidic channels, without the involvement of chiral agents. The flow induces the formation of periodic chiral structures caused by director field bending and elastic instability. The direction and periodicity of these structures depend on flow velocity and channel geometry.

Another example involves the induction of enantiomeric excess in prochiral azobenzene dimers under CPL [41]. Photoisomerization occurs with a slight predominance of one enantiomer, which over time leads to the accumulation of chiral excess.

The controlled synthesis of chiral and achiral isomers of 3D metal-organic frameworks (MOFs) from achiral tectons is presented in [42]. Chirality induction was achieved by varying growth conditions and employing enantiopure agents. X-ray structural analysis confirmed the presence of double helices in chiral MOFs. Chirality did not originate from the intrinsic properties of molecules but emerged through self-assembly in a confined environment. These 3D polymers exhibit enhanced thermal stability and spin transitions sensitive to external factors, making them promising candidates for the development of adaptive functional materials.

**Beta Decay (Asymmetric Weak β-Radiation)**

Asymmetric β-radiation, particularly from isotopes such as $^{14}C$ and $^{60}Co$, is a source of spin-polarized electrons with a defined chiral orientation, arising from parity violation in weak interactions. This phenomenon was first experimentally confirmed by Chien-Shiung Wu et al. [43], who demonstrated that β-electrons emitted by the $^{60}Co$ isotope exhibit spins

predominantly oriented opposite to the nuclear spin. In the 1960s, it was hypothesized that such spin-polarized electrons could selectively degrade one enantiomer of chiral molecules through interaction with circularly polarized bremsstrahlung radiation [1]. In 2014, Joan Dreiling [44] experimentally showed that bombardment of 3-bromocamphor with spin-polarized electrons results in more efficient destruction of one enantiomer [45].

Enantioselective transfer of the rotational state of chiral molecules (1-indanol) was implemented in [46], achieving 96% enantiomeric purity. The method employs precisely tuned microwave fields to excite molecular rotations, opening new prospects in spectroscopy, quantum information, and parity violation measurements.

Sources of γ-radiation, such as $^{60}$Co, as well as ionization chambers with chiral surfaces (e.g., quartz), are employed for the radiolysis of chiral molecules. Thermal transport has been observed in chiral insulating quartz [47], driven by phonons with angular momentum sensitive to the CISS effect. This phenomenon may explain macroscopic chirality transfer through spin interactions. It has been found that such phonons can induce spin polarization associated with CISS. Specifically, CISS may enhance the generation of phonon spin angular momentum, and its long-range transfer could account for the macroscopic CISS effect observed at room temperature. In the device designed for thermal transport measurements, the quartz supporter is mounted on a copper thermal bath with a 2 mm deep groove for thermal contact, while a resistor tip acting as an electric heater is placed on the upper surface of the supporter, as shown in Fig. 3a.

The irradiation of $\beta^-$-pinene with γ-rays from $^{60}$Co is described in [48], which, instead of causing racemization, resulted in the formation of a polymer with enhanced optical activity. This phenomenon is interpreted as chiral amplification and is considered one of the possible mechanisms underlying the emergence of homochirality on early Earth.

## CHIRALITY AND CLUSTEROLUMINESCENCE

A significant contribution to understanding the mechanisms of chirality generation was made in [49], where the relationship between aggregation processes and the emergence of chiral signals in luminescent molecules was studied. Specifically, three types of systems were examined, exhibiting two opposing phenomena: aggregation-induced circular dichroism (AICD) and aggregation-annihilated circular dichroism (AACD). In the case of AICD, the focus was on molecules with aggregation-induced emission (AIE compounds) functionalized with chiral fragments such as amino acids or sugar residues. These molecules showed no optical activity in solution; however, upon transitioning to an aggregated state, they displayed a pronounced circular dichroism (CD) signal. This demonstrates that chirality can be transferred from localized chiral sites to chromophores through intermolecular interactions within aggregates. It was established that right-handed (P) helices are associated with a negative Cotton effect in CD spectra, whereas left-handed (M) helices correspond to a positive effect. Conversely, AACD was observed in systems with axial chirality (e.g., biaryl structures), manifesting as the disappearance or attenuation of the chiral signal in the aggregated state. This annihilation of chirality was shown to result from changes in the dihedral angle between aromatic rings, specifically, a reduction in rotational angles that diminishes the chirality of the macromolecular structure.

The obtained results indicate that aggregation not only affects the physicochemical properties of substances but can also act as a trigger for the generation or suppression of chiral information. Therefore, molecular interactions in the supramolecular state are capable of modulating chiral properties even in initially achiral systems. This opens new opportunities for the development of functional chiral materials, including optically active sensors, materials for chiral spintronics, as well as novel approaches to understanding stereogenesis under both natural and synthetic conditions.

Chirality is a fundamental property of molecules that determines their asymmetry and ability to engage in stereoselective interactions. In biological systems, chirality underlies molecular recognition, enzymatic activity, and pharmacological specificity. Recent studies have demonstrated that chiral effects can influence not only biological activity but also the physicochemical properties of substances, particularly photoluminescence and chirality-induced spin selectivity (CISS effect) [50, 51].

Fluorescence spectroscopy enables the observation of spin-dependent effects during the interaction of chiral molecules with magnetized supporters. For instance, the photoluminescence of nanoparticles bound to ferromagnetic supporters via chiral oligopeptides varies depending on the orientation of the external magnetic field. Similar observations have been reported for spin-dependent electron [52] and energy transfer [53]. In donor-bridge-acceptor systems, where the chirality of the bridge plays

a crucial role, it has been demonstrated that excitation of the donor part with circularly polarized light can induce spin-selective charge transfer to the chiral acceptor [54].

A new photophysical phenomenon, such as clusteroluminescence, has gained particular significance, as its discovery has broadened our understanding of luminescence sources. Clusteroluminescence occurs in non-conjugated systems such as heteroatomic polymers, amino acids, or polypeptides, where electron delocalization arises from intermolecular *n*–π*-overlap within densely packed aggregates [55-57].

Unlike classical luminescence, which requires conjugated π-systems, clusteroluminescence is observed in the solid state or at high concentrations in solution, where molecules form dense associates with effective interatomic overlap. This phenomenon explains light emission by many non-conjugated substances, including polyethylene glycols, amino acids, polyamides, polyurethanes, and biopolymers (e.g., polypeptides) [56, 58]. Particularly intriguing is the dependence of clusteroluminescence on chirality, as demonstrated in polypeptides such as polylysine. It has been established that racemic polypeptides exhibit significantly higher fluorescence intensity than their homochiral counterparts. This is attributed to the fact that the incorporation of amino acids with opposite chirality disrupts the ordered β-helical structure and promotes the formation of a random coil conformation, which allows carbonyl groups to interact more effectively in space, forming fluorescently active clusters [58].

Clusteroluminogenic systems have a broad range of applications: from optoelectronics (in light-emitting diodes and displays) to biomedicine (as probes, sensors, and imaging markers), as well as in information security and environmental monitoring [59].

Ultimately, the relationship between chirality and cluster luminescence opens new approaches for designing functional materials with controllable optical properties. The combination of CISS, AIE, and clusteroluminescence effects creates a new class of materials in which optical activity is governed by spatial organization and stereochemistry. This approach holds significant potential for applications in spintronics, stereoselective diagnostics, quantum technologies, and advanced sensor platforms [60].

Chirality plays a fundamental role in biosystems and nanomaterials, determining the specificity of molecular recognition, information transfer, and optical activity. Of particular importance is the transmission of chiral information in self-assembled systems capable of luminescence, especially circularly polarized luminescence (CPL). The design of a positively charged chiral π-building block containing an AIE-active GluCN fragment is presented in [61]. This block can self-assemble into nanostructures of various dimensional morphologies (0D-nanospheres, 2D-nanoplates, and 3D-nanocubes) and generate CPL emission. Special attention was given to how dimensional morphology influences selective chirality and energy transfer within the system involving achiral dyes ThT (positively charged) and CNA (negatively charged). It was found that only 2D-nanoplates can transfer chirality to CNA while simultaneously enabling efficient energy transfer, thereby enhancing the CPL signal. In contrast, 3D- and 0D-structures did not exhibit such properties, demonstrating the critical role of morphology in nanostructure functionality. These findings reveal that morphology-controlled nanostructures can serve as tools for fine-tuning optical activity and information exchange at the nano- and molecular levels. This work deepens our understanding of chirality and energy transfer mechanisms in artificial systems, bringing them closer to the complexity of natural bioenvironments and opening new prospects for chiroptical materials, sensor technologies, and polarized light-harvesting devices.

A novel approach to designing chiral luminescent materials with aggregation-induced emission (AIE) was proposed in [62] based on structural modification of the axially chiral (R)-BINOL framework. Instead of the conventional attachment of AIE-active fragments to chiral sites, the authors integrated 2-substituted furans directly into the BINOL structure. This strategy overcame the strong aggregation-induced quenching inherent to this compound and its small Stokes shift, enabling the development of new fluorophores with pronounced solid-state emission properties, improved photostability, thermal stability, and tunable emission wavelength. The key to success was the creation of molecules with an overall distorted geometry and bulky substituents that effectively prevent π–π-stacking in the solid state, thereby promoting high fluorescence efficiency (Fig. 4).

Circular dichroism spectroscopy confirmed the successful transfer of chirality from BINOL to the newly developed AIE compounds, particularly for samples S3 and S4. These luminogens proved not only optically active but also biocompatible: S4 exhibited a high quantum yield, a significant Stokes shift, and stable accumulation in the cytoplasm of

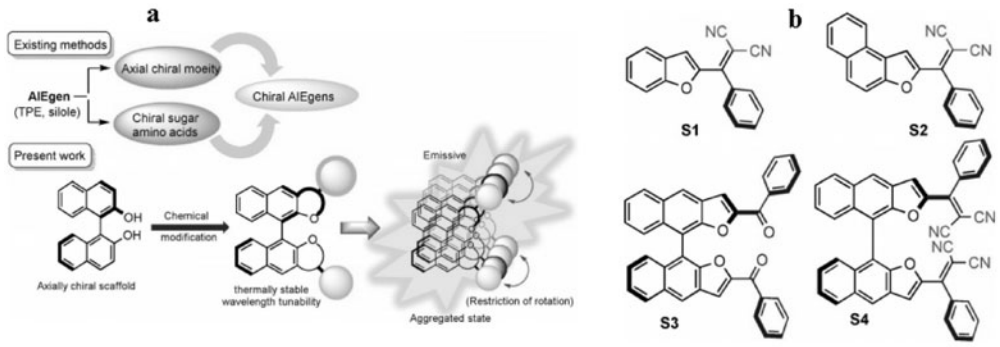


Fig. 4. Rational design of chiral AIE compounds (a), Structures of the developed AIE compounds S1-S4 (b). Reproduced and adapted from [62] with permission of © 2006 Wiley-VCH Verlag GmbH & Co. KGaA.

MDA-MB-231 cancer cells, confirming its effectiveness as a fluorescent probe. Thus, the proposed strategy enables the creation of chiral AIE-active materials without external luminescent fragments, opening new prospects for the development of advanced bio-probes and optoelectronic systems with controllable optical properties.

In [63], emphasis is placed on the potential of chiral AIE compounds (aggregation-induced emission luminogens) for visualizing and monitoring the dynamics of phase interfaces. In particular, the use of circularly polarized luminescence (CPL) is considered an advanced method for capturing chiral processes in real time. It was found that the twisted structure of AIE compounds, especially tetraphenylethylene (TPE) derivatives, can impart intrinsic chirality even in the absence of external chiral inducers. Several examples demonstrate how blocking TPE rotation or encapsulating it within cubic structures preserves chirality in solution and generates intense CPL signals. This opens new opportunities for creating self-chiral fluorophores suitable for monitoring phase boundaries, especially where conventional methods such as electron microscopy are inadequate. In this context, the combination of AIE and CPL is regarded as a novel strategy for visualizing chiral changes and symmetry breaking at different interfaces.

Axially chiral bisbenzocoumarins were synthesized for the first time in [64] by modifying 1,1′-binaphthol (BINOL), where the naphthol fragments were transformed into benzocoumarin rings. The resulting compounds, particularly (R)-BBzC1 and (S)-BBzC1, exhibit not only aggregation-induced emission (AIE) but also unique chiral effects, including aggregation-annihilated circular dichroism (AACD) (Fig. 5).

Special emphasis was placed on the dependence of chiral optical properties on the nature of substituents at 3,3′-positions of the binaphthol framework. It was established that substitution with ester groups in BBzC1 promotes the occurrence of AACD, in particular, the disappearance of the circular dichroism signal in the aggregated state. This effect is explained by a reduction in the dihedral angle between benzocoumarin rings during aggregation, which influences configurational stability and chiral transfer. X-ray structural analysis of the (*R*)-BBzC1 monocrystal confirmed the presence of a large dihedral angle that prevents π-π-stacking between molecules, thereby facilitating AIE while simultaneously creating conditions for dynamic attenuation of the chiral signal upon aggregation. The use of two BBzC1 enantiomers allowed tracking the influence of chirality not only in solution but also in the solid state. It was found that fluorescence in dilute solutions is suppressed due to intramolecular rotation, whereas restricted motion enhances emission in the aggregated state. At the same time, changes in the chiral environment of molecules during aggregation lead to hypsochromic shifts and weakening of the CD signal, which is direct evidence of chirality annihilation through conformational changes. This study not only demonstrated the photophysical and chiral properties of new axially chiral AIE-active coumarin materials but also revealed an important correlation between substituents, molecular geometry, and chirality behavior in the aggregated state. The obtained results provide a foundation for further rational design of chiral light-emitting materials, particularly those with controllable circular dichroism.

The self-assembly of axially chiral bisbenzocoumarins (BB) and their ability to recognize small chiral molecules, particularly 1-phenylethanol (PE), was studied in [65]. It was established that decreasing the polarity of the medium promotes

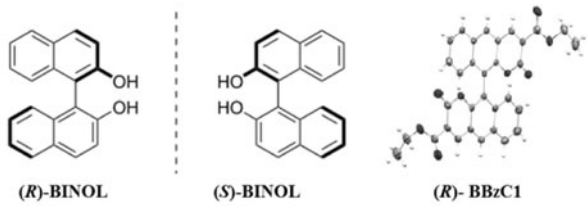


Fig. 5. Structures of (*R*)-BINOL, (*S*)-BINOL, and (*R*)-BBzC1. Adapted from [64] with permission of © 2017 Elsevier.

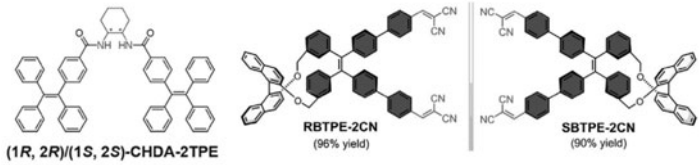


Fig. 6. (1R,2R)/(1S,2S)-CHDA-2TPE [66] (adapted with permission of © 2025 Elsevier) and RBTPE-2CN, and SBTPE-2CN [67].

H-type aggregation of DB, forming ordered supramolecular structures. Special attention was given to the chiral interaction between BB and PE, which proved to be the most pronounced among the three tested chiral molecules. Circular dichroism (CD) spectra recorded signal changes indicative of induced conformational rearrangement of BB in the presence of PE. Chemical modeling analysis revealed that this rearrangement is associated with an increase in the dihedral angle between the aromatic fragments of BB, caused by π–π-stacking with PE. Thus, the study demonstrates selective chiral recognition of PE by BB in solution, supported by both experimental and theoretical data. The proposed approach may serve as a basis for developing new chirality-sensitive recognition systems, which is important for analytical chemistry, biosensors, and pharmaceuticals.

Enantioselective recognition is critically important in pharmaceutical quality control and biochemical analysis. However, in practice, it remains a challenging task due to the subtle differences between enantiomers. Two new chiral fluorescent probes, namely, (1R,2R)-CHDA-2TPE and (1S,2S)-CHDA-2TPE, were developed in [66] by combining cyclohexanediamine (which imparts chirality) with tetraphenylethylene (TPE), a classical AIE-active fragment (Fig. 6).

These probes retained the typical aggregation-induced emission (AIE) capability, allowing them to exhibit fluorescence only in the aggregated state, thereby reducing background signals in solution. The use of these probes demonstrated pronounced enantioselectivity toward 11 chiral reagents, including amino acids and organic acids. A particularly striking example involves L- and D-glutamic acid, where up to an 88.8-fold difference in fluorescence intensity was observed between the respective enantiomers. This indicates the probe's ability not only to detect the presence of a molecule but also to distinguish its spatial configuration. The recognition mechanism was confirmed by spectroscopic methods, notably $^{1}$H NMR titration, which revealed the formation of hydrogen bonds as a key factor in the specific interaction between the probe and the target enantiomer. The recognition principle operates via a "fluorescence turn-on" mechanism: probe aggregation occurs in the presence of only one enantiomer, resulting in an intense fluorescence signal. Overall, the developed chiral probes combine structural simplicity with high sensitivity and selectivity, making them effective tools for quantitative and qualitative determination of enantiomeric purity in solutions. This approach holds significant potential for applications in the pharmaceutical industry, bioanalytics, and chiral control in synthetic chemistry.

A modular synthetic strategy was presented in [67] for creating materials with circularly polarized luminescence (CPL) across the entire visible spectrum, based on chiral macrocyclic luminogens exhibiting aggregation-induced emission (AIE). This was achieved through molecular engineering and variation of acceptor fragments, enabling the development of a series of solid-state chiral AIE compounds with tunable emission colors. Four pairs of such AIE compounds were synthesized, maintaining high quantum yields in the solid state and displaying CPL emission from blue to red in various environments: as nanoaggregates, in liquid-crystalline matrices, and in polymer films. Samples RBTPE-2CN and SBTPE-2CN, containing

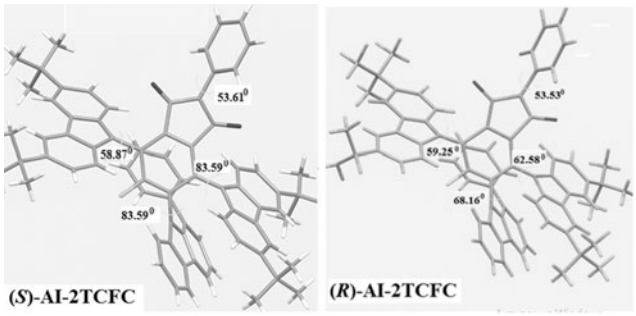


Fig. 7. X-ray crystal structure of the racemic compound (rac)-AI-2TCFC and the corresponding dihedral angle ([68]).

strong acceptor fragments, exhibited characteristics of intramolecular charge transfer and solvatochromism, as well as AIE behavior at high water content. Structural identification, quantum-chemical calculations (DFT/TD-DFT), and chiral HPLC analysis confirmed the chiral geometry and purity of the synthesized compounds. Mirror-image CPL emission and CD signals were observed, varying with intermolecular π–π-packing and aggregate structure type. Additional tuning of CPL color was achieved by adjusting the polarity of the polymer matrix. This study demonstrates that donor-acceptor engineering combined with modulation of chiral structure enables the creation of CPL-active materials with customized emission colors. According to this approach, ongoing work aims to develop chiral AIE compounds for the near-infrared region.

A new strategy for synthesizing chiral materials with circularly polarized luminescence (CPL) based on axial C–N bond chirality was proposed in [68]. This approach effectively utilized the chromophoric properties of nitrogen-containing heterocycles, particularly carbazole, as a structural element for constructing the chiral framework. An enantiomeric pair of chiral emitters, (S)-AI2TCFC and (R)-AI2TCFC (Fig. 7), was synthesized, exhibiting a luminescence peak at 578 nm in toluene and in the solid state. Both compounds display aggregation-induced emission, thermally activated delayed fluorescence, and luminescence dissymmetry factors ($g_{lum}$) of $+1.3\cdot10^{-3}$ and $-8.5\cdot10^{-4}$. The $g_{lum}$ factor is defined as $g_{lum} = 2(I_L - I_R)/I_L + I_R$, where $I_L$ and $I_R$ are the intensities of left- and right-circularly polarized emission, respectively. The theoretical maximum $g_{lum} = 2$ corresponds to fully circularly polarized emission.

Small energy gaps between singlet and triplet states ($\Delta E_{ST} = 0.03$ eV) and a high reverse intersystem crossing rate ($k_{RISC} = 8.59\cdot10^5$ $s^{-1}$) were achieved due to steric hindrance and intramolecular π–π-interactions. The materials were successfully tested in circularly polarized organic light-emitting diodes (CP-OLEDs), demonstrating excellent electroluminescent performance. Thus, the proposed C–N axial chirality expands existing approaches to the design of CPL-active materials and provides a platform for new optoelectronic applications.

Review [69] focuses on recent advances in the development of materials with circularly polarized luminescence (CPL) based on chiral liquid crystals (LCs) and liquid-crystalline polymers. Particular attention is given to the role of chirality in self-organized, orientationally ordered soft systems capable of generating CPL. Various types of chiral LCs are discussed, including thermotropic cholesteric LCs, bent-core LCs, and lyotropic LCs based on nanocellulose or polyacetylene. Significant emphasis is placed on chiral LC-polymer structures, such as helical nanofibers and networks, which exhibit enhanced CPL stability and enable control over luminescence dissymmetry ($g_{lum}$).

It has been shown that integrating chiral domains with inorganic nanoparticles, such as perovskites, enables the creation of structures with $g_{lum}$ values up to 1.9. Special attention is given to the self-assembly of bent-core molecules in the presence of chiral additives, which form chiral supernanospaces capable of efficiently generating CPL. The review also outlines specific chiral architectures that provide modulated CPL responses across a broad spectral range, from ultraviolet to terahertz. The effects of π-π-interactions, axially chiral fluorophores, and photonic band gaps are demonstrated as strategies for achieving CPL sign inversion and controlling its intensity. A separate section addresses the challenge of increasing $|g_{lum}|$ values toward the theoretical maximum ($g_{lum} \to 2$). The review emphasizes the need for new mechanisms, materials, and processing technologies to create CPL-active structures with high efficiency, long-term stability, and tunable emission wavelengths. Thus,

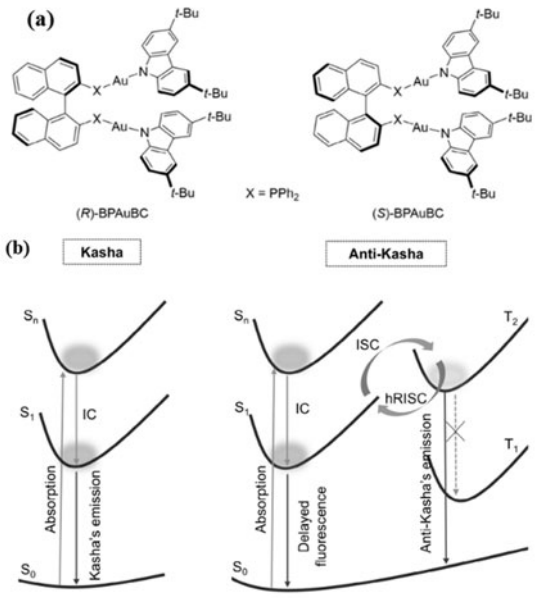


Fig. 8. Structural formula of enantiomers of gold complexes ((R)- and (S)-BPAuBC) (a); schematic representation of Kasha emission (left), anti-Kasha phosphorescence from $T_2$ (right), and delayed fluorescence via a high-level reverse intersystem crossing (hRISC) process activated by stabilization of the high-lying triplet excited state $T_2$ (right) (b) ([70]).

chiral liquid-crystalline systems emerge as a promising platform for synthesizing CPL-active materials with tailored optical properties for applications in optics, photonics, biotechnology, and quantum communication.

A novel chiral strategy for designing highly efficient materials with circularly polarized luminescence (CPL) was developed in [70], based on the use of axial chirality. Synthesized enantiomers of gold complexes ((R)- and (S)-BPAuBC) (Fig. 8a), combining axially chiral binaphthyl skeletons with 3,6-di-tert-butylcarbazole fragments, exhibit a strong CPL response due to ordered helical packing in the solid state. The key chiral effect in this study is aggregation-induced CPL (AI-CPL), which occurs in the crystalline environment through stable chiral molecular conformation and efficient transfer of chiral information. The luminescence dissymmetry factor ($g_{lum}$) significantly increases upon transition from solution to solid state, as confirmed by X-ray diffraction analysis.

Additionally, a unique feature of these chiral systems lies in their ability to utilize high-energy triplet states ($T_2$) instead of the conventional first excited triplet state ($T_2$), thereby violating Kasha's rule (Fig. 8b). This enables intense circularly polarized delayed fluorescence through high-energy reverse intersystem crossing (hRISC), representing an innovative approach in CPL photophysics. Such an effect is possible due to the presence of a chiral framework that stabilizes electronic states and facilitates selective transitions between them. Another significant achievement in chiral technologies is the controlled acid-base switching of CPL emission in nanoparticles, opening prospects for the development of intelligent chiral sensors and highly responsive CPL-active devices. Overall, this study demonstrates that axial chirality embodied in the binaphthyl skeleton is a powerful tool for designing CPL materials with high $g_{lum}$ values, expanding the scope of excited-state manipulation and laying the foundation for the advancement of next-generation chiral optoelectronics.

## CHIRAL MINERALS AND INORGANIC NANOMATERIALS

Chiral mineral surfaces, such as left- and right-handed quartz, can enantioselectively adsorb amino acids, promoting the formation of enantiomeric excess (e.g., L-alanine on l-quartz and D-alanine on d-quartz) [71]. Such surfaces influence

crystallization selectivity [72], photochemical processes [30], and can transfer chirality to achiral molecules in CPL systems [73]. Chiral induction in iodate minerals ($KIO_3$ and $LiIO_3$) under the influence of amino acids was demonstrated in [74], accompanied by morphological changes and enantioselective adsorption. The chirality of these systems was confirmed by circular dichroism and LFR methods.

Chiral gold nanomaterials (CGNMs) represent a novel class of inorganic materials with promising applications in optoelectronics, sensor technologies, and catalysis [75]. The synthesis of such systems relies on controlled morphology, surface functionalization, and the spontaneous emergence of chirality without chiral ligands, as exemplified by the $Au_{102}$(p-MBA)$_{44}$ nanoparticle featuring a well-defined chiral lattice [76]. CGNMs exhibit CPL activity, enantioselective catalytic behavior, and high biocompatibility. A significant difference in the dissociation of L- and D-cysteine on the chiral copper surface Cu{421}R has been reported in [77], confirmed by spectroscopic analysis and quantum-chemical calculations based on density functional theory (DFT). The prospects of CGNMs are linked to dynamically controlled chirality and require a synergistic approach integrating DFT, molecular dynamics, and artificial intelligence.

## CHIRALITY-INDUCED SPIN SELECTIVITY: MECHANISMS AND APPLICATIONS IN ELECTROCATALYSIS

Chirality-induced spin selectivity (CISS) is a quantum-mechanical phenomenon whereby chiral molecules can selectively conduct electrons with a specific spin orientation. Remarkably, this occurs even in the absence of an external magnetic field, indicating the intrinsic ability of chirality to directly influence electron spin [78, 79]. The CISS effect was first reported in studies by Ron Naaman's group and has since become the subject of extensive theoretical and experimental studies [80, 81]. The emission of spin-polarized photoelectrons from an Au(111) surface coated with double-stranded DNA clearly demonstrated the role of the chiral DNA polymer in generating a response to circularly polarized light [50].

The essence of the CISS effect lies in the fact that electron transport through chiral molecules exhibits asymmetry: electrons with one spin orientation pass with a higher probability than those with the opposite orientation [82]. This phenomenon arises from the spatial asymmetry of chiral structures, which influences their interaction with electron spin [83]. The CISS effect is associated with differences in electron transmission probabilities depending on their spin state during passage through chiral molecules [84]. At the macroscopic level, this leads to spin polarization of the current even in the absence of a magnetic field. Quantum interference effects also make a significant contribution to the CISS mechanism, as electrons behave simultaneously as waves and particles. In such cases, the interaction of electronic wave functions can be either constructive or destructive depending on spin, resulting in selective polarization [85]. The arrangement of atoms within a chiral molecule, as well as the electronic structure of its excited states, is also critical for the manifestation of the CISS effect [86]. Additional contributions to the mechanism arise from quantum effects such as spin-orbit coupling [87, 88], particularly the geometry and curvature of the electron-bond chain within the molecular structure along the electron transfer pathway, momentum changes, and structural asymmetry.

One of the earliest practical applications of the CISS effect was the detection of radiation-induced DNA damage [89]. This approach enables the identification of even minor modifications in the helical structure due to its high sensitivity to changes in molecular symmetry. For instance, spin selectivity allows reliable detection of DNA lesions induced by UV irradiation.

The hydrogen evolution reaction (HER) is one of the most common cathodic processes in industrial electrochemical applications [50, 90, 91]. In 2015, it was first demonstrated that deposition of chiral molecules on the anode surface enhances HER performance [90]. Peptides (Al5, A17) and DNA were employed in comparison with achiral analogs. Chiral-modified anodes required lower overpotentials and exhibited higher hydrogen generation rates. Subsequent studies [91] utilized anodes incorporating CdSe quantum dots within a conductive polymer, further amplifying the effect. Thus, chiral materials not only reduce HER overpotential but also improve efficiency in photoelectrocatalytic systems through the CISS mechanism.

Human respiration relies on the oxygen reduction reaction (ORR) [87], which is central not only to aerobic life [90] but also to fuel cells [50, 92] and other clean energy technologies. The ORR mechanism is inherently complex because the reaction is spin-forbidden: the ground electronic state of molecular oxygen is a triplet ($^3\Sigma g^-$), whereas the products of the enzymatic

reaction of $O_2$ with glucose ($H_2O$, $CO_2$) exist in singlet electronic states with closed shells [93-97]. Clearly, the subtleties of the biochemical mechanism of respiration remain understudied [87, 88].

The CISS mechanism can enhance the efficiency not only of the oxygen reduction reaction (ORR) but also of the oxygen evolution reaction (OER) – both remain critical bottlenecks in numerous electrochemical and electrocatalytic processes, including water electrolysis, ion-exchange membranes in batteries, fuel cells, and more [50, 92, 98]. Electrocatalytic water splitting has long been considered a cost-effective and promising method for hydrogen production [50, 92]. CISS is particularly promising for improving OER, which traditionally suffers from high energy barriers. It has been established that the spin state of electrons significantly influences the OER pathway, as triplet $O_2$ requires spin coordination [92].

According to [99-101], the use of chiral coatings or intrinsically chiral materials can reduce the Tafel slope, suppress $H_2O_2$ formation, and facilitate electron transfer through spin-selective pathways. For instance, a chiral $Fe_3O_4$ film inhibited the formation of the $H_2O_2$ byproduct, lowered the potential required to achieve a current density of 10 mA/cm$^2$ by 150 mV, reduced the Tafel slope to 104 mV/dec, increased current density by 42% at 1.8 V (relative to the saturated calomel electrode, SCE), decreased charge-transfer resistance by 50%, enabled a tenfold increase in free charge carrier density, and prolonged electron lifetime within the catalyst [50, 99].

For example, Ni-doped 2D $MoS_2$ layers with intrinsic chirality demonstrated significant improvement in OER performance [98, 102]. In experiments, the Tafel slope decreased from 105 to 60 mV/dec, while $H_2O_2$ formation was reduced threefold. It was also shown that the intrinsic chirality of the crystal lattice has a greater impact than external coatings. A chiral mesostructure of Co-doped nickel oxide (L-Co-NiO) was developed in another study [103], exhibiting long-term stability (960 h) and high open-circuit voltage (OCV, 1.57 V) in zinc-air batteries.

CISS also demonstrates significant potential for ORR. A CSAFePc system, chiral-modified iron phthalocyanine, was developed, in which chiral peptides act as axial ligands and spin filters. The best performance was achieved with the D-enantiomer, exhibiting an initial ORR potential of 1.01 V in an alkaline medium [104]. These findings highlight the feasibility of employing chiral self-assembled systems based on non-precious metals in fuel cells. High activity and selectivity are achieved through spin polarization induced by chirality.

Electroreduction of $CO_2$ to valuable $C_2^+$ products remains a challenging task, particularly for metals other than copper. However, CISS has enabled the activation of silver as a catalyst for C–C-bond formation [105]. The use of chiral silver nanofilms (CNAF), synthesized with phenylalanine, allowed the production of ethylene, ethane, propane, ethanol, and acetic acid, achieving a total Faradaic efficiency of 4.7% and a current density of 22 mA/cm$^2$. Chirality facilitated spin alignment of ethylene dione in the triplet state *OCCO, which is essential for C–C-bond formation. This opens a new pathway for electrocatalysis without relying on Cu.

CISS has also been implemented in hybrid $MoS_2$ layers, where chirality is introduced via methylbenzylamine [98]. The resulting systems exhibited spin polarization of up to 75% and significantly enhanced OER activity. The combination of organic chirality and inorganic conductivity creates highly efficient electrocatalytic materials for PEC/EC systems and spintronics.

## HOMOCHIRAL SUBSTRATE OR CATALYST

The formation of homochirality may have been influenced by external factors such as circularly polarized light from astrophysical sources, asymmetric β-radiation (e.g., from $^{14}C$ or $^{60}Co$), and chiral minerals, such as quartz or iron-nickel compounds, that selectively adsorb enantiomers [106-108].

Autocatalytic reactions, including Frank's model (1953) [106] and the Soai reaction [107-110], illustrate how an initial enantiomeric excess can self-amplify to homochirality. The Soai reaction, based on the alkylation of pyrimidinecarbaldehyde with diisopropylzinc, is a unique example of absolute asymmetric synthesis, where chirality emerges from achiral components without any external chiral source.

According to [111], the Soai reaction embodies two fundamental principles of life, such as self-replication and homochirality. The effect can be initiated even by weak asymmetries (such as circularly polarized light or chiral crystals) and

demonstrates biological relevance [112]. Furthermore, Viedma's experiments [113] revealed that grinding mixtures of chiral crystals ($NaClO_3$) in the presence of glass beads leads to the system's transition to complete homochirality, even without initial asymmetry, due to autocatalytic recrystallization. This underscores the possibility of spontaneous symmetry breaking in physical systems.

## SELF-DISPROPORTIONATION OF ENANTIOMERS

In the context of chiral separation, considerable attention has traditionally been devoted to methods based on chiral environments, such as catalysts, sorbents, or reagents. However, recent advances have demonstrated the feasibility of efficiently separating enantiomers even under achiral conditions through the phenomenon of self-disproportionation of enantiomers (SDE). This phenomenon relies on differences in the physicochemical behavior of scalemic mixtures (partially enantiomer-enriched) during separation processes, particularly in achiral chromatography. Such an approach opens new prospects for scalable, reproducible, and economically viable purification of chiral compounds without the need for expensive chiral components.

Two recent review articles explore cutting-edge approaches to the purification of chiral compounds [114] and the role of fluorine-containing chiral pharmaceuticals [115]. Particular attention is devoted to the phenomenon of self-disproportionation of enantiomers (SDE), an innovative method for separating scalemic mixtures without the use of chiral stationary phases. The efficiency of this approach has been confirmed under achiral chromatography conditions using simulated moving bed (SMB), enabling high enantiomeric purity (up to 99% *ee*) with excellent productivity and reproducibility. Furthermore, an analysis of newly approved fluorinated chiral drugs over the past five years revealed a wide range of architectures of fluorinated molecules with varying numbers of stereocenters, significantly influencing their biological activity. The reviews emphasize the need for further study of SDE in the context of fluorinated chiral compounds, given its potential for developing more efficient purification technologies. The authors also highlight environmental risks associated with fluorine accumulation and underscore the strategic importance of fluorinated chiral structures in the design of next-generation pharmaceuticals.

## CHIRAL PHOTOCATALYSIS AND PHOTOCATALYTIC PROCESSES

The growing interest in the role of chirality in photochemical reactions has driven active research in chiral photocatalysis, both in fundamental and applied contexts. Particular attention is devoted to photocatalytic processes capable of enabling enantioselective transformations, including the synthesis of valuable organic products, isolation of enantiomers from racemic mixtures, removal of pollutants from textile and pharmaceutical wastewater, as well as applications in biomedical studies. Currently, homogeneous systems have been most extensively studied in the field of asymmetric catalysis, where the active components are molecular photocatalysts of various types, namely, low-molecular-weight organic and inorganic compounds, metal complexes, polymers, and others. It should be noted that in many studies on asymmetric catalysis, photocatalytic reactions encompass both processes based on photophysical stages, namely, photoexcitation followed by energy transfer (i.e., sensitization), and reactions involving electron transfer after photoexcitation, generating radical species and subsequent transformations mediated by these intermediates.

A kinetic model was proposed in [116] that integrates the synthesis of enantiomer-enriched amino acids with autocatalytic peptide ligation capable of chiral amplification. It also discusses the role of homochirality in RNA/DNA as a precursor to protein chirality.

According to [117], homochiral polypeptides form more stable and compact structures than heterochiral ones, as confirmed by both lattice and atomic-level modeling. This finding is significant for the design of synthetic proteins and xenobiochemistry.

Xeno amino acids and their potential role in the emergence of alternative forms of life were examined in [118]. Particular attention is given to chirality as one of the factors in evolutionary selection. These examples illustrate how photocatalysis in a chiral environment could have promoted the selective formation or preservation of L-amino acids, bringing us closer to understanding the origin of biological homochirality.

**Chirality in 2D Covalent Organic Frameworks (COFs): Homochiral vs. Racemic Structures.** Chiral covalent organic frameworks (CCOFs) are promising porous materials with potential applications in enantioselective separation. Current synthetic strategies (post-synthetic modification, direct synthesis, and chiral induction) and their uses in chromatography, membranes, and sorption were summarized in [119]. It emphasizes the need for scalable synthesis methods, topology optimization, and the integration of computational modeling. Homochiral and racemic 2D COFs based on [5]helicenes were compared in [120]. Homochiral COFs form asymmetric hexagonal structures with pronounced chiroptical properties (Cotton effect up to 800 nm), whereas racemic COFs exhibit higher structural order but lower optical activity. This work confirms the critical role of absolute stereochemistry in determining COF structure and functionality, extending the Liebisch-Wallach rule to organic 2D systems.

An essential prerequisite for efficient enantioselective photocatalytic transformations is the positioning of the substrate within a chiral environment after its binding as a complex with a chiral photocatalyst. Such complexes may include tight van der Waals associates, donor-acceptor complexes, or assemblies stabilized by hydrogen bonding. For example, 3-allyl-substituted quinolones were converted under visible light into 3-cyclopropyl quinolones (88-96%, 32-55% *ee* yield ) in the presence of a chiral thioxanthone sensitizer capable of forming hydrogen bonds [121]. An intramolecular [2+2] photocycloaddition was achieved in a 4-butenyloxy-2-quinolone molecule in deuterated chloroform at –70°C using a triplet sensitizer based on benzophenone bearing chiral substituents capable of hydrogen bonding with the substrate, [122]. According to the proposed mechanism, quinolone binds to the chiral sensitizer as a ground-state complex, where light-induced energy transfer occurs from benzophenone to the associated quinolone. The cycloaddition proceeds within the chiral microenvironment of a host-guest-type complex, forming a secondary complex, namely a cycloadduct, whose dissociation regenerates the sensitizer and releases the chiral product containing a cyclobutane ring.

[2+2] Photocycloaddition in 3-alkoxyquinolones has been achieved with high yield and enantioselectivity (up to 98% yield, up to 91% *ee*) using a series of chiral iridium complexes incorporating pyridyl-pyrazole ligands in their coordination sphere [123]. Experimental studies employing $^{1}$H NMR spectroscopy and theoretical calculations revealed that substrate binding to the iridium complex occurs through π–π-interactions and an unusual hydrogen bond between the quinolone amide group and the pyrazole fragment of the ligand. The proposed photocycloaddition mechanism involves energy transfer from the triplet excited state of the iridium complex to the quinolone substrate.

A chiral rhodium photocatalyst was employed for asymmetric dearomatization in methanolic solutions of various benzofurans and benzothiophene functionalized with an N-acyl pyrazole fragment [124]. The reaction, carried out in the presence of styrenes substituted by different groups, led to chiral photocycloaddition products with high yields and enantioselectivity (up to 91% yield, up to 99% *ee*) [124]. According to the proposed mechanism, the process begins with the formation of a complex between the chiral rhodium photocatalyst and the acylpyrazole substrate. Upon irradiation with a blue LED, the complex transitions to a singlet and subsequently to a triplet excited state. Interaction of the triplet complex with the styrene substrate generates an intermediate biradical, which ultimately leads to the formation of the final chiral cyclobutane product.

Highly enantioselective photocatalytic α-aminoalkylation of acyclic imine derivatives has been achieved in a homogeneous system using a chiral bisoxazoline copper(II) complex [125]. In the proposed mechanism, copper complexes perform multiple functions: as a Lewis acid, activating imine by entering the coordination sphere of the copper(II) complex; generating photoactive copper(I) particles and the α-aminoalkyl radical via single-electron oxidation of amine; inducing asymmetry during the radical addition to the C=N double bond in the copper(II)–imine complex; and reducing the intermediate through the photoexcited copper(I) complex. The process concludes with protonation and ligand exchange, releasing the chiral diamine product and regenerating the copper(II)–imine complex.

A homogeneous system based on a tandem photocatalyst (chiral iridium complex/chiral phosphoric acid) was employed to carry out highly enantioselective [2+2] photocycloaddition involving various vinylpyridines and styrene, yielding chiral pyridine-substituted cyclobutane products (up to 95% yield, up to 95% *ee*) [126]. It was established based on studies of the influence of system components on absorption and luminescence spectra that the components exhibit minimal interaction in

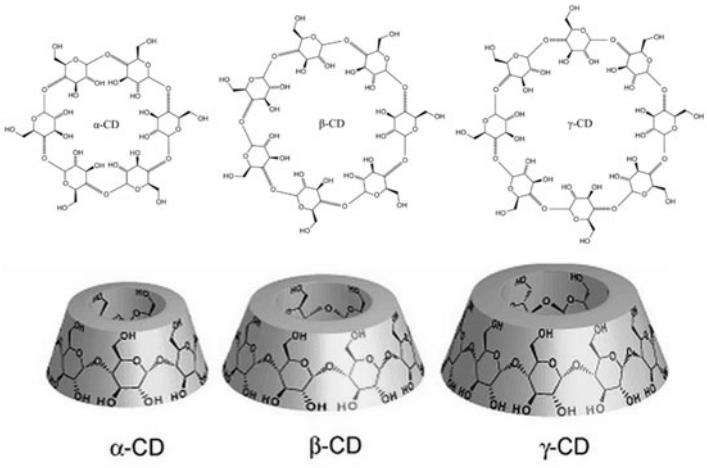


Fig. 9. Molecular structure of three principal cyclodextrins ([128]).

the ground state, and the photochemical process proceeds via a transient complex formed upon interaction between the photoexcited iridium sensitizer and the chiral phosphoric acid.

Macromolecular systems capable of encapsulating small organic molecules and influencing their chemical transformations have found application in asymmetric photocatalytic synthesis [127, 128]. Cyclodextrins (CDs) occupy a special position among them, namely, cyclic oligosaccharides with a hollow truncated cone structure, exhibiting a unique ability for complex formation and widely utilized in chemistry and biotechnology. Natural D-CDs have long been employed; however, their mirror-image L-analogues remained inaccessible. The synthesis of α-, β-, and γ-L-cyclodextrins based on L-glucopyranose was achieved for the first time in [129, 130] with high stereoselectivity. The chirality of L-CDs was confirmed by X-ray diffraction analysis, induced electronic circular dichroism, and vibrational circular dichroism, where a characteristic band at 1150 $cm^{-1}$ was observed, associated with chirality-sensitive C–O bond vibrations. This opens possibilities for their selective excitation by circularly polarized IR radiation. Studies revealed the ability of L-CDs to undergo chiral self-sorting in the solid state, specific enantiomer recognition (e.g., fenchone by α-L-CD), and enzymatic stability due to their non-recognition by enzymes. They hold promise for the development of CPS-active systems, MOFs, sensors, chiral catalysts, mechanically interlocked molecules, and chiral chromatography. Prospects include the synthesis of L-CDs using mirror-image biocatalysts, further expanding their functional potential in stereoselective chemistry, materials science, and biomedical applications.

Cyclodextrins are classified as α-CD (6 subunits), β-CD (7 subunits), and γ-CD (8 subunits) (Fig. 9) depending on the number of glucose subunits in their structure.

An example of cyclodextrin application in the production of chiral compounds involves the enantioselective photocyclodimerization of 2-anthracenecarboxylic acid (AC) in the presence of γ-CD as a chiral template [131, 132]. The components form a 1:2 inclusion complex in the ground state in the initial reaction mixture. Upon irradiation, several isomeric cyclic products are generated, such as syn- and anti-dimers of the “head-to-tail” (HT) and “head-to-head” (HH) types. Their distribution primarily depends on the mutual orientation of AC molecules within the γ-CD cavity (Fig. 10), since during photoexcitation, changes in their orientation are impossible due to steric constraints.

An enantiopure tetrahedral coordination cage constructed from 4,40-diamino-biphenyl-2,20-disulfonic acid and 2-formylpyridine with iron(II) was also employed as a photocatalyst for the [4+4] photocyclodimerization of 2-anthracenecarboxylate (AC) in an aqueous medium [134]. According to studies, one AC molecule partially entered the small cavity of the cage through hydrophobic interactions, while the second was bound to the biphenyl fragment at the cage periphery via π-stacking interactions. Irradiation of this system resulted in the formation of AC dimers, namely, syn-HT and anti-HH, with enantiomeric excess values of 14% and 4%, respectively.

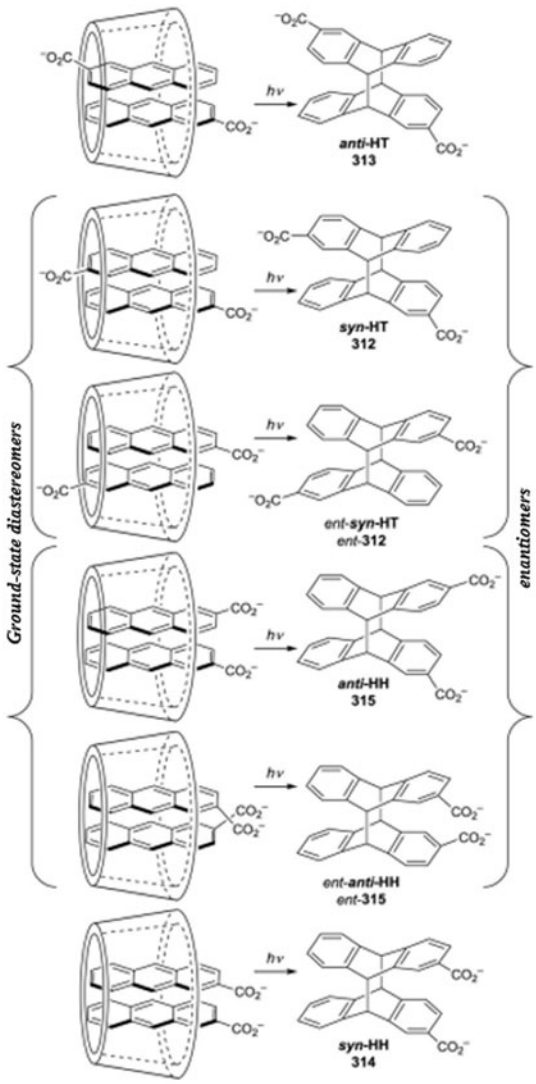


Fig. 10. Possible orientations of anthracenecarboxylate molecules within the γ-CD cavity and the structure of products formed via [4+4] photodimerization. Reproduced from [133] with permission of © 2022 American Chemical Society.

Although various homogeneous photocatalytic systems for asymmetric synthesis have already been studied, several obstacles remain on the path to the practical implementation of such processes. The main challenges include the need to obtain typically complex chiral photocatalysts, the use of nonpolar organic solvents that facilitate the formation of reagent-photocatalyst associates, difficulties in isolating reaction products, and the inability to reuse the photocatalyst. Consequently, increasing attention in the field of asymmetric catalysis has recently shifted toward heterogeneous systems based on solid-state chiral materials. Compared to homogeneous systems, these offer advantages such as ease of product separation, catalyst regeneration, and generally high stability, which supports the development of continuous large-scale technologies for producing desired chiral products.

Different substances can serve as solid-state chiral photocatalysts for asymmetric synthesis. An example of an organic photocatalyst includes a conjugated microporous polymer network based on cross-linked poly(benzothiadiazole), synthesized via the cross-coupling of 4,7-dibromobenzo[c][1,2,5]thiadiazole with 1,3,5-triethynylbenzene [135]. This material,

functioning as an organic semiconductor with a band gap of $E_g$ = 2.4 eV, was employed to carry out stereoselective [2+2] cycloaddition reactions involving (E)-1-methoxy-4-(prop-1-en-1-yl)benzene (trans-anethole) and styrene derivatives under visible-light irradiation, yielding a series of cyclobutane derivatives.

Tandem photocatalytic systems based on two 3D covalent organic frameworks (COFs) containing a photoredox triphenylamine fragment, in the presence of a chiral imidazolidinone catalyst developed by MacMillan, were employed for asymmetric α-alkylation of aldehydes [136]. The COFs were obtained using triangular and rectangular precursors connected via condensation between tetrakis(4-aminophenyl)ethene and 4′,4‴,4⁗,4⁗′-nitrilotris(([1,1′-biphenyl]-4-carbaldehyde)) (COF-1), and between tris(4-aminophenyl)amine and 4′,4‴,4⁗,4⁗′,4⁗′′′′-(ethene-1,1,2,2-tetrayl)tetrakis{[(1,1′-biphenyl)-4-carbaldehyde]} (COF-2). Enantioselective α-alkylation of a series of aldehydes under blue-light irradiation proceeded efficiently using both photocatalytic systems, affording yields of 51-88% and enantiomeric excess values of 83-94%.

Efficient photocatalytic enantioselective α-alkylation of aldehydes was also achieved in systems based on two organic semiconductors, namely, covalent organic frameworks (QH-COFs) incorporating tetrahydroquinoline groups [137]. The organic frameworks were synthesized in a one-step process in the presence of scandium and ytterbium trifluoromethanesulfonates ($Sc(OTf)_3$/$Yb(OTf)_3$) as Lewis acid catalysts, via cascade condensation and cycloaddition reactions between 1,3,5-tris(*p*-formylphenyl)benzene and benzidine (QH-COF-1) and ethyl vinyl ether, or between 1,3,5-tris(*p*-formylphenyl)benzene with 1,3,5-tris(4-aminophenyl)benzene, and ethyl vinyl ether (QH-COF-2). QH-COFs proved to be stable materials under acidic/basic conditions and upon light irradiation. Alkylation of *n*-butyraldehyde with 2-bromoacetophenone was performed using these frameworks under blue-light irradiation in the presence of MacMillan's chiral imidazolidinone catalyst and 2,6-dimethylpyridine (QH-COF-1: product yield of 75%, *ee* of 91%; QH-COF-2: product yield of 60%, *ee* of 91%). Chiral products were also formed with high efficiency when using various substituted 2-bromoacetophenones and other bromine-containing compounds as substrates (see Table 1).

Chiral coordination polymers, or metal-organic frameworks (MOFs), represent promising heterogeneous photocatalysts for asymmetric synthesis. Specifically, enantiomeric zinc-containing MOFs (Zn-PYI1 and Zn-PYI2) incorporating a photoredox triphenylamine fragment and a stereoselective organocatalyst, L- or D-pyrrolidine-2-imidazole (PYI), were synthesized and demonstrated high photocatalytic activity in the asymmetric α-alkylation of aliphatic aldehydes [138]. The MOFs were prepared via a solvothermal reaction between 4,4′,4′′-tricarboxytriphenylamine and $Zn(NO_3)_2{\cdot}6H_2O$ in the presence of L/D-N-tert-butoxycarbonyl-2-(imidazole)-1-pyrrolidine, followed by thermal treatment to remove tert-butoxy groups. The corresponding chiral products in high yields (Zn-PYI1: 65-84%, *ee* 86-92%; Zn-PYI2: 61-85%, *ee* 78-99%) were obtained upon irradiation with a standard fluorescent lamp of solutions of diethyl 2-bromomalonate with phenylpropyl aldehyde, octaldehyde, or unsaturated (E)-nonaldehyde in the presence of MOFs and lutidine.

Inorganic semiconductor materials have also been employed as active components in systems for photocatalytic asymmetric synthesis and transformation of chiral compounds. For instance, chiral mesostructured ZnS nanospheres (CMZ), composed of arrays of helical nanorods obtained via a hydrothermal method using L- or D-cysteine, exhibited photocatalytic activity in the enantioselective synthesis of amino acids through $CO_2$ reduction in the presence of $NH_3$ [139]. Among the identified products were serine with an enantiomeric excess exceeding 96%, glycine, alanine, and other amino acids. The chiral structure of ZnS facilitated spin polarization, promoting the separation of photogenerated charge carriers and the formation of triplet ethylene dione particles $^3$OCCO and other intermediates via C–C bond formation between $C_2$ and $C_1$ particles, ultimately yielding 3-hydroxypyruvic acid and final products, such as amino acids.

Current data on the synthesis, structure, and physicochemical properties of chiral perovskites of various dimensionalities (from 0D to 3D) were reviewed and analyzed in [140]. Their optical and electrical characteristics, as well as potential applications in optoelectronics, spintronics, and nonlinear optics, are discussed. An analysis of organic chiral compounds that can serve as ligands for the synthesis of three-dimensional chiral perovskites is provided. Special attention is given to the possibility of using chiral dyes to enhance the optical properties of hybrid perovskite systems.

Hybrid nanostructured photocatalysts based on $CsPbBr_3$ perovskite modified with chiral 1-phenylethylamine demonstrated high enantioselective activity (with enantiomeric excess up to 99% and yields up to 72%) in the visible-light-driven oxidation of a series of N-arylamines, producing the corresponding N-C axially chiral N-heterocycles, namely, N-arylindoles [141], which are present in many natural products and are highly important as precursors for

TABLE 1. Catalytic Performance of Different Types of Photocatalysts in Asymmetric α-alkylation of Aldehydes [137]

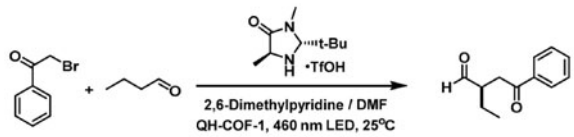


| Photocatalyst | Yield[a], % | *ee*[b], % |
|---|---|---|
| None | N.D.[c] | – |
| QH-COF-1[d] | N.D. | – |
| THQ | N.D. | – |
| QH-COF-1 | 75 | 91 |
| COF-1 | 30 | 84 |
| QH-COF-2 | 60 | 91 |
| $[Ru(bpy)_3]Cl_2·6H_2O$[e] | 80 | 91 |
| $BiVO_4$ | 20 | 91 |
| $WO_3$ | 18 | 88 |
| $TiO_2$ (P25) | 27 | 91 |
| QH-COF-1 (TEMPO)[f] | <3 | – |
| QH-COF-1 (DIPEA)[g] | <3 | – |

**Note**. Reaction conditions: 2-bromoacetophenone (0.809 mmol), *n*-butyraldehyde (1.62 mmol), 2,6-dimethylpyridine (1.62 mmol), triflate salt of (2R,5S)-2-tert-butyl-3,5-dimethylimidazolidin-4-one (0.162 mmol), photocatalyst (30 mg), anhydrous DMF (2 mL), irradiation with blue LEDs (30 W) for 12 h. [a] Yield of isolated product based on bromide; [b] determined by $^1$H NMR analysis of diastereomeric acetals obtained via derivatization with (2S,4S)-2,4-pentanediol; [c] not detected; [d] light off; [e] $[Ru(bpy)_3]Cl_2·6H_2O$ (8.09 μmol); [f] TEMPO (1.62 mmol); [g] DIPEA (1.62 mmol).

pharmaceuticals. The developed systems employing chiral metal-halide perovskite nanocrystals enabled the synthesis of both R- and S-indole enantiomers when using chiral perovskites R- or S-PEA/$CsPbBr_3$, respectively. Mechanistic studies combining experimental methods and quantum-chemical modeling revealed that the chiral surface of the photocatalyst plays a key role in ensuring enantioselectivity by binding the molecule of the prochiral substrate or the intermediate oxidation product of the N-arylamine.

Chiral quantum dots $Cu_{2-x}S$, obtained by reacting $CuCl_2$ with thiourea in the presence of D-penicillamine (QD $Cu_{2-x}S$-L) or L-penicillamine (QD $Cu_{2-x}S$-D), were employed as photocatalysts for protein cleavage, using bovine serum albumin (BSA) as a model [142]. The highest activity was exhibited by $Cu_{2-x}S$-L quantum dots under irradiation with left-hand polarized visible light, which may be attributed both to stronger binding of BSA to the $Cu_{2-x}S$-L surface and to the generation of a greater number of hot electrons and highly reactive OH radicals. Chiral cadmium telluride nanoparticles, synthesized by passing gaseous hydrogen telluride into a solution of $Cd(ClO_4)_2$ containing D- or L-cysteine and glutathione (GSH) as a stabilizer, upon photoexcitation, demonstrated the ability to cleave a specific site in a 90-base-pair double-stranded DNA

molecule, as well as to perform sequence-specific DNA cleavage in live animal cells *in vivo* [143]. According to studies, this property of cysteine-modified chiral nanoparticles is associated with their high affinity for a specific 90-base-pair DNA sequence and the formation of reactive oxygen species (primarily OH radicals) responsible for DNA cleavage.

Chiral nanoparticles D/L-$Fe_xCu_ySe$, obtained by functionalizing $Fe_xCu_ySe$ nanoparticles with D- or L-type penicillamine (Pen), demonstrated high efficiency in inhibiting the aggregation of monomeric Aβ42 peptide molecules under near-infrared irradiation [144], a key component of amyloid plaques, which is a hallmark of Alzheimer's disease. D-$Fe_xCu_ySe$ nanoparticles exhibited greater activity than L-$Fe_xCu_ySe$ due to their significantly higher affinity for Aβ42 fibrils. Moreover, they more effectively promoted the conversion of Aβ42 fibrils into looser monomers and enhanced fibril disaggregation as a result of generating a larger amount of reactive oxygen species. *In vivo* experiments confirmed that D-$Fe_xCu_ySe$ nanoparticles help protect neurons from damage caused by Aβ42 deposition and alleviate symptoms in a mouse model of Alzheimer's disease.

Composite silver-containing chiral plasmonic photocatalysts Ag@$TiO_2$ [145] and Ag/AgCl@$TiO_2$ [146], prepared using helical $TiO_2$ nanofibers synthesized with N-stearoyl-D-glutamic acid as a template, demonstrated photocatalytic activity in the degradation of the synthetic hormone 17α-ethinylestradiol (EE2), a contaminant of aquatic environments. The efficiency of EE2 degradation depended on the size of silver nanoparticles and the length of chiral $TiO_2$ nanofibers [145]. The process rate was maximal at an average silver particle size of ~12-14 nm and when using the longest helical $TiO_2$ particles, which is attributed to achieving optimal conditions for enhancing the surface plasmon resonance effect under visible-light irradiation. The mechanism involves the injection of photoexcited electrons from silver nanoparticles into the $TiO_2$ conduction band, followed by their capture by $O_2$ molecules to form reactive oxygen species ($O_2^{-\bullet}$, $OH^{\bullet}$), which ultimately lead to EE2 degradation.

In conclusion, only selected examples of the application of various types of materials for the production of chiral compounds, which are important for pharmaceuticals and biomedical uses, as well as for the detoxification of chiral substances that act as environmental pollutants, have been considered here.

## CONCLUSION

Chiral molecular systems found in living organisms (proteins, lipids, carbohydrates, DNA, and RNA) are strictly homochiral. Although the chemical behavior of two enantiomers may be similar, their bioactivity often differs dramatically. Despite identical chemical formulas, the three-dimensional structure of enantiomers determines their interaction with circularly polarized light. This manifestation of chirality has long been known and widely applied in structural chemistry and biochemistry. The discovery by Ron Naaman in 2006 of the link between chirality and spin-magnetic effects paved the way for a new era in the natural sciences related to the study of matter structure. It was established that chirality at the level of molecules, polymers, and solids is associated with electron spin and, consequently, with the dipolar structure of the magnetic field. The curvature of magnetic field lines shows an analogy with the helical structure of chiral molecules such as DNA or polypeptides, realized through spin-orbit interaction, in particular, a quantum effect arising during the translational motion of an electron along a chiral electrostatic potential. The phenomenon of chirality-induced spin selectivity has been experimentally confirmed in numerous chemical processes and is now actively studied in the context of spintronics, catalysis, and biophysics.

**Acknowledgements** The authors express their sincere gratitude to S. Ya. Kuchmiy for valuable advice, scientific discussion, and assistance in preparing the section devoted to chiral photocatalysis. His contribution was instrumental in enhancing the scope and depth of the topic's presentation in the article.

**Author contributions** T. V. Sakhno: supervision, writing, editing. B. P. Minaev: discussion of results, general editing. Y. E. Sakhno: writing and discussion.

Funding This work was performed without financial support.

**Conflict of interest** The authors declare no conflict of interest.

**REFERENCES**


1. Q. Sallembien, L. Bouteiller, J. Crassous, and M. Raynal, *Chem. Soc. Rev*., **51**, 3436-3476 (2022), https://doi.org/10.1039/D1CS01179K.
2. A. D. Garcia, C. Meinert, H. Sugahara, et al., *Life*, **9**, 29 (2019), https://doi.org/10.3390/life9010029.
3. I. Mejdrova, E. Wegrzyn, and T. Carell, *Chem. Asian J.*, **20**, e202401074 (2025), https://doi.org/10.1002/asia.202401074.
4. M. Fiore, *Symmetry*, **17**, 473 (2025), https://doi.org/10.3390/sym17030473.
5. G. Yang, S. Zhang, J. Hu, et al., *Symmetry*, **11**, 474 (2019), https://doi.org/10.3390/sym11040474.
6. A. G. Griesbeck, and U. J. Meierhenrich, *Angew. Chem. Int. Ed*., **41**, 3147-3154 (2002).
7. W. A. Bonner, E. Rubenstein, *Biosystems*, **20**, 99-111 (1987).
8. K. Michaeli, N. Kantor-Uriel, R. Naaman, and D. H. Waldeck, *Chem. Soc. Rev*., **45**, 6478-6487 (2016).
9. B. Minaev, *Arch. Pulmonol. Respir. Care*, **8,** No. 1, 028-033 (2022), https://doi.org/10.17352/aprc.000081.
10. J. Bailey, *Orig. Life Evol. Biosph*., **31**, 167-183 (2001), https://doi.org/10.1023/A:1006751425919.
11. F. Ozturk and D. Sasselov, *Proc. Natl. Acad. Sci. U.S.A*., **119**, e2204765119 (2022), https://doi.org/10.1073/pnas.2204765119.
12. A. Rodger and D. Marshall, *Biochem. (Lond.),* **43**, No. 2, 58-64 (2021), https://doi.org/10.1042/bio_2020_105.
13. W. R. Kitzmann, J. Freudenthal, A.-P. M. Reponen, et al., *Adv. Mater*., **35**, 2302279 (2023), https://doi.org/10.1002/adma.202302279.
14. U. Meierhenrich, *Amino Acids and the Asymmetry of Life. Caught in the Act of Formation*, Series Advances in Astrobiology and Biogeophysics, Springer, Berlin, Heidelberg (2008).
15. G. Longhi, E. Castiglioni, J. Koshoubu, et al., *Chirality*, **28**, 696-707 (2016). https://doi.org/10.1002/chir.22647.
16. P. Della Sala, C. Talotta, M. De Rosa, et al., *J. Am. Chem. Soc.*, **147**, No. 24, 20843-20854 (2025), https://doi.org/10.1021/jacs.5c04512.
17. D. Ayuso, A. F. Ordonez, and O. Smirnova, *Phys. Chem. Chem. Phys*., **24**, 26962-26991 (2022).
18. X. Gao, J. Wang, K. Yang, et al., *Chem. Mater*., **34**, 6116-6128 (2022).
19. R. U. McVicker, and N. M. O'Boyle, *J. Med. Chem*., **67**, 2305-2320 (2024).
20. M. M. Green, and V. Jain, *Orig. Life Evol. Biosph*., **40**, 111-118 (2010).
21. L.-T. Deck, M. S. Hosseinalipour, and M. Mazzotti, *J. Am. Chem. Soc*., **147**, No. 22, 18826-18839 (2025).
22. A. Berthod, *Anal. Chem*., **78**, 2093-2099 (2006).
23. A. Hagelschuer, D. Padin, V. Daskova, and B. L. Feringa, *J. Am. Chem. Soc*., **147**, 18662-18673 (2025).
24. J. Bailey, A. Chrysostomou, J. H. Hough, et al., *Science*, **281**, No. 5377, 672-674 (1998).
25. J. Bailey, *Orig. Life Evol. Biosph*., **31**, 167-183 (2001).
26. D. P. Glavin, and J. P. Dworkin, *Origins Life Evol. Biosph*., **39**, 261-273 (2009).
27. M. Fujiki, *Possible Scenarios for Homochirality on Earth*, MDPI eBooks, Basel, 2019. https://doi.org/10.3390/BOOKS978-3-03921-723-6.
28. A. C. Evans, C. Meinert, C. Giri, et al., *Chem. Soc. Rev*., **41**, 5447-5458 (2012), https://doi.org/10.1039/C2CS35051C.
29. P. De Marcellus, C. Meinert, M. Nuevo, et al., *Astrophys. J. Lett*., **727**, L27 (2011).
30. T. Kawasaki, M. Sato, S. Ishiguro, et al., J. Am. Chem. Soc., **127**, No. 10, 3274-3275 (2005).
31. R. Hadidi, D. K. Bozanic, H. Ganjitabar, et al., *Commun. Chem*., **4**, 72 (2021).
32. M. Tia, B. C. de Miranda, S. Daly, et al., *J. Phys. Chem. Lett*., **4**, 2698-2704 (2013).
33. Y. Takano, J.-I. Takahashi, T. Kaneko, et al., *Earth Planet. Sci. Lett*., **254,** Nos. 1-2, 106-114 (2007).
34. F. Mortaheb, K. Oberhofer, J. Riemensberger, et al., *Angew. Chem. Int. Ed*., **58**, No. 44, 15685-15689 (2019).
35. R. D. Tremblay, R. Amos, and R. Kobayashi, *Astron. Comput*., **46**, 100791 (2024).
36. C. Zhang, X. Wang, and L. Qiu, *Front. Chem*., **9**, 711488 (2021).
37. U. J. Meierhenrich, J.-J. Filippi, C. Meinert, et al., *Chem. Biodivers*., **7**, 1651-1659 (2010).
38. D. P. Glavin, J. E. Elsila, A. S. Burton, et al., *Meteorit. Planet. Sci*., **47**, 1347-1364 (2012), https://doi.org/10.1111/j.1945-5100.2012.01400.x.
39. J. M. Ribo, J. Crusats, F. Sagues, et al., *Science*, **292**, 2063-2066 (2001).

40. Q. Zhang, W. Wang, S. Zhou, et al., *Nat. Commun*., **15**, 7 (2024).
41. R. K. Rijeesh, P. K. Hashim, S.-I. Noro, and N. Tamaoki, *Chem. Sci*., **6**, 973-980 (2015).
42. Y.-T. Yang, B.-Y. Jin, Y. Chai, et al., *Chem. Mater*., **37**, 3363-3372 (2025).
43. C. S. Wu, E. Ambler, R. W. Hayward, et al., *Phys. Rev*., **105**, 1413-1415 (1957).
44. J. M. Dreiling, *Asymmetric interactions between spin-polarized electrons and chiral molecules*, Ph.D. Dissertation, University of Nebraska – Lincoln, ProQuest Dissertations & Theses (2014), 3618568.
45. J. M. Dreiling, F. W. Lewis, and T. J. Gay, *J. Phys. B.* **51**, 21LT01 (2018), https://doi.org/10.1088/1361-6455/aae1bd.
46. J. Lee, E. Abdiha, B. G. Sartakov, et al., *Nat. Commun*. **15**, 7441 (2024).
47. K. Ohe, H. Shishido, M. Kato, et al., *Phys. Rev. Lett*. **132**, 056302 (2024).
48. F. Cataldo, and Y. Keheyan, *Radiat. Phys. Chem*. **75**, 572-582 (2006).
49. H. Zhang, R. T. K. Kwok, J. W. Y. Lam, and B. Z. Tang, *Proceedings of SPIE - The International Society for Optical Engineering*, 10735 (2018).
50. B. P. Bloom, Y. Paltiel, R. Naaman, and D. H. Waldeck, *Chem. Rev*., **124**, 1950-1991 (2024).
51. P. C. Mondal, P. Roy, D. Kim, et al., *Nano Lett*., **16**, 2806-2811 (2016).
52. J. M. Abendroth, N. Nakatsuka, M. Ye, D. Kim, et al., *ACS Nano*, **11**, 7516-7526 (2017).
53. P. Roy, N. Kantor-Uriel, D. Mishra, et al., *ACS Nano*, **10**, 4525-4531 (2016).
54. B. P. Bloom, B. M. Graff, S. Ghosh, et al., *J. Am. Chem. Soc*., **139**, 9038-9043 (2017).
55. T. V. Sakhno, Yu. E. Sakhno, and S. Ya. Kuchmiy, *Theor. Exp. Chem*., **58**, 297-327 (2022).
56. T. V. Sakhno, Yu. E. Sakhno, and S. Ya. Kuchmiy, *Theor. Exp. Chem*., **59**, 75-106 (2023).
57. Q. Fan, Y. Tang, H. Sun, et al., *Adv. Mater*., 2401315 (2024).
58. W. Zhao, M. Gao, L. Kong, et al., *Biomacromolecules*, **25**, 1897-1905 (2024).
59. T. Sakhno, D. Ivashchenko, A. Semenov, et al., *Low Temp. Phys*., **50**, 276-287 (2024).
60. V. M. Granchak, T. V. Sakhno, I. V. Korotkova, et al., *Theor. Exp. Chem*., **54**, 147-177 (2018).
61. L. Ji, Y. Zhao, M. Tao, et al., *ACS Nano*, **14**, No. 2, 2373-2382 (2020).
62. V. P. Jejurkar, G. Kumar, R. Srivastava, and S. Saha, *Chem. Eur. J.,* **27**, No. 17, 5470-5482 (2021).
63. H. Zhang, J. Z. Sun, J. Liu, and B. Z. Tang, *J. Appl. Phys*., **126** 050901 (2019), https://doi.org/10.1063/1.5110688.
64. S. Chen, L. Wei, Z. Ge, et al., *Spectrochim. Acta A*, **193**, 141-146 (2018).
65. H. Zhang, Y. Li, Y. Lu, Y. Ming, et al., *Dyes Pigments*, **216,** 111325 (2023), https://doi.org/10.1016/j.dyepig.2023.111325.
66. C. Qi, Q. Li, K. Wei, et al., *Dyes Pigments*, **239**, 112781 (2025), https://doi.org/10.1016/j.dyepig.2024.112781.
67. Y. Li, J. Liang, S. Fu, et al., *Aggregate,* **5**, e613 (2024), https://doi.org/10.1002/agt2.613.
68. L. Zeng, C.-H. Guo, C. Li, et al., *Aggregate*, **0**, e70069 (2025), https://doi.org/10.1002/agt2.70069.
69. J. Liu, Z.-P. Song, L.-Y. Sun, et al., *Responsive Mater.*, **1***,* e20230005 (2023), https://doi.org/10.1002/rpm.20230005.
70. K. Wang, X. Ou, X. Niu, et al., *Aggregate*, **6***,* e667 (2025), https://doi.org/10.1002/agt2.667.
71. D. Avnir, *Minerals*, **14**, No. 10, 995 (2024), https://doi.org/10.3390/min14100995.
72. U. J. Meierhenrich, L. Nahon, C. Alcaraz, et al., *Angew. Chem. Int. Ed.*, **44**, No. 35, 5630-5634 (2005), https://doi.org/10.1002/anie.200501311.
73. R.-H. Jin, S. Tsunega, T. Nakashima, and T. Kawai, *ChemPlusChem*, **85**, No. 4, 619-626 (2020), https://doi.org/10.1002/cplu.201900615.
74. M. Oliel, and Y. Mastai, *Nanoscale Adv.*, **7**, 2599 (2025), https://doi.org/10.1039/D4NA00879D.
75. K. Soai, T. Kawasaki, and A. Matsumoto, *Symmetry*, **11**, 694 (2019), https://doi.org/10.3390/sym11050694.
76. P. D. Jadzinsky, G. Calero, C. J. Ackerson, et al., *Science*, **318**, 430-433 (2007), https://doi.org/10.1126/science.1149859.
77. M. J. Gladys, K. M. O'Donnell, A. Tadich, et al., *J. Phys. Chem. C*, 123, 20829-20837 (2019), https://doi.org/10.1021/acs.jpcc.9b03373.
78. S.-J. Zheng, H. Chen, S.-Q. Zang, and J. Cai, *Matter*, **8**, No. 2, 101924 (2025), https://doi.org/10.1016/j.matt.2024.11.018.
79. K. Chae, N. A. R. C. Mohamad, J. Kim, et al., *Chem. Soc. Rev.*, **53**, 9029-9058 (2024).
80. K. Ray, S. P. Ananthavel, D. H. Waldeck, and R. Naaman, *Science*, **283**, 814-816 (1999).

81. Z. Hanne, R. Naaman, and H. Zacharias, *Science*, **331**, 894-897 (2011).
82. R. Naaman, Y. Paltiel, and D. H. Waldeck, *J. Phys. Chem. Lett*., **11**, 3660-3666 (2020).
83. A. Chiesa, M. Chizzini, E. Garlatti, et al., *J. Phys. Chem. Lett*., **12**, 6341-6347 (2021).
84. R. Naaman, and D. H. Waldeck, *Annu. Rev. Phys. Chem*., **66**, 263-281 (2015).
85. S. Chen, and H.-H. Fu, *J. Phys. Chem. Lett*., **14**, No. 49, 11076-11083 (2023).
86. M. S. Zollner, A. Saghatchi, V. Mujica, and C. Herrmann, *Chem. Theory Comput*., **16**, No. 2, 7357-7371 (2020).
87. Y. Sang, F. Tassinari, K. Santra, et al., *PNAS*, **119**, No. 30, e2202650119 (2022).
88. B. Minaev, Biomed. *J. Sci. Tech. Res*., **38**, 30462-30472 (2021).
89. N. Bangruwa, M. Srivastava, and D. Mishra, *ACS Omega*, **7**, 37705-37713 (2022).
90. W. Mtangi, V. Kiran, C. Fontanesi, and R. Naaman, *J. Phys. Chem. Lett*., **6**, 4916-4922 (2015).
91. F. Tassinari, K. Banerjee-Ghosh, F. Parenti, et al., *J. Phys. Chem. C*, **121**, 15777-15783 (2017).
92. D. Barik, U. Utkarsh, and K. Banerjee Ghosh, *Chem. Commun*., **61**, 6226-6245 (2025).
93. B. F. Minaev, N. A. Murugan, and H. Agren, *Int. J. Quantum Chem*., **113**, No. 14, 1847-1867 (2013), https://doi.org/10.1002/qua.24390.
94. B. F. Minaev, and V. A. Minaeva, *Phys. Chem. Chem. Phys*., **3**, No. 5, 720-729 (2001), https://doi.org/10.1039/b006712l.
95. B. P. Minaev, T. V. Sakhno, O. O. Panchenko, and Y. E. Sakhno, *Theor. Exp. Chem*., **60**, No. 2, 91-107 (2024).
96. B. F. Minaev, *J. Appl. Spectroscopy,* **42** (5), 518-523 (1985), https://doi.org/10.1007/BF00661398.
97. B. F. Minaev, and H Agren. *Collect. Czech. Chem. Commun*. **60**, No. 3, 339-371 (1995). https://doi.org/10.1135/cccc19950339.
98. Z. Bian, K. Kato, T. Ogoshi, et al., *Adv. Sci*., **9**, 2201063 (2022).
99. W. Zhang, C. Jiang, H. Guan, et al., *Mater. Adv*., **5**, 1340-1347 (2024).
100. S. Ma, H. Lee, and J. Moon, *Adv. Mater*., **36**, 2405685 (2024).
101. Z. Xue, B. Wu, Z. Zhang, et al., *ACS Catal*., **14**, 5685-5695 (2024).
102. D. Zabelin, A. Tulupova, P. Svec, et al., *J. Power Sources*, **641**, 236839 (2025), https://doi.org/10.1016/j.jpowsour.2025.236839.
103. Y. S. Park, J. Lee, H. Lee, et al., *ACS Appl. Mater. Interfaces*, **17**, 18228-18242 (2025), https://doi.org/10.1021/acsami.4c04053.
104. L. Scarpetta-Pizo, R. Venegas, P. Barrias, et al., *Angew. Chem*., **136**, e202315146 (2024). https://doi.org/10.1002/ange.202315146.
105. W. Zhang, J. Ai, T. Ouyang, et al., *J. Am. Chem. Soc*., **146**, 28214-28221 (2024). https://doi.org/10.1021/jacs.4c08445.
106. F. C. Frank, *Biochim. Biophys. Acta*, **11**, 459-463 (1953),
107. K. Soai, T. Shibata, H. Morioka, and K. Choji, *Nature*, **378**, 767-768 (1995).
108. K. Soai, A. Matsumoto, and T. Kawasaki, *Adv. Asym. Autocat. Relat. Top*., 1-30 (2017), https://doi.org/10.1016/B978-0-12-812824-4.00001-0.
109. D. G. Blackmond, *Chem. Rev*., **120**, 4831-4847 (2020), https://doi.org/10.1021/acs.chemrev.9b00557.
110. D. G. Blackmond, *Proc. Natl. Acad. Sci. U.S.A*., **101**, 5732-5736 (2004).
111. K. Soai, *Tetrahedron*, **124**, 133017 (2022).
112. K. Soai, T. Kawasaki, and A. Matsumoto, *Orig. Life Evol. Biosph*., **52**, 57-74 (2022).
113. C. Viedma, *Phys. Rev. Lett*., **94**, 065504 (2005).
114. A. Wzorek, K. Klika, J. Han, et al., *Ukr. Chem. J*., **91**, 34-48 (2025).
115. J. Han, A. Wzorek, G. Dhawan, et al., *Ukr. Chem. J*., **91**, 55-90 (2025).
116. P. G. Higgs, and D. G. Blackmond, *Proc. Natl. Acad. Sci. U.S.A*., **122**, e2423683122 (2025).
117. V. Nanda, A. Andrianarijaona,and C. Narayanan, *Protein Sci*., **16**, 1667-1675 (2007).
118. S. M. Brown, C. Mayer-Bacon, and S. Freeland, *Life*, **13**, 2281 (2023), https://doi.org/10.3390/life13122281.
119. M. Cheng, S. Zhou, Y. Kuang, et al., *Coord. Chem. Rev*., **542**, 216844 (2025), https://doi.org/10.1016/j.ccr.2025.216844.
120. J. del R. Monroy, T. Deshpande, J. Schlecht, et al., *J. Am. Chem. Soc*., **147**, 17750-17763 (2025), https://doi.org/10.1021/jacs.5c01004.

121. A. Troster, A. Bauer, C. Jandl, and T. Bach, *Angew. Chem. Int. Ed*., **58**, 3538-3541 (2019), https://doi.org/10.1002/anie.201814193.
122. D. F. Cauble, V. Lynch, and M. J. Krische, *J. Org. Chem*., **68**, 15-21 (2003). https://doi.org/10.1021/jo020630e.
123. K. L. Skubi, J. B. Kidd, H. Jung, et al., *J. Am. Chem. Soc*., **139**, 17186-17192 (2017), https://doi.org/10.1021/jacs.7b10586.
124. N. Hu, H. Jung, Y. Zheng, et al., *Angew. Chem. Int. Ed*., **57,** 6242-6246 (2018), https://doi.org/10.1002/anie.201802891.
125. B. Han, Y. Li, Y. Yu, and L. Gong, *Nat. Commun*., **10**, 3804 (2019), https://doi.org/10.1038/s41467-019-11688-7.
126. S. J. Chapman, W. B. Swords, C. M. Le, et al., *J. Am. Chem. Soc*., **144**, 4206-4213 (2022), https://doi.org/10.1021/jacs.2c00063.
127. M. Morimoto, S. M. Bierschenk, K. T. Xia, et al., *Nat. Catal.,* **3**, 969-984 (2020), https://doi.org/10.1038/s41929-020-00528-3.
128. M. Rao, W. Wu, and C. Yang, *Green Synth. Catal*., **2**, 131-144 (2021), https://doi.org/10.1016/j.gresc.2021.03.005.
129. Y. Wu, S. Aslani, H. Han, et al., Y. Qiu, *Nat*. *Synth*., **3**, No. 6, 698-706 (2024).
130. D. W. Armstrong, S. Aslani, J. Nafie, et al., *J. Am. Chem. Soc*., **5**, No. 2, 693-701 (2025).
131. Y. Nakamura, and Y. Inoue, *J. Am. Chem. Soc*., **125**, 966-972 (2003), https://doi.org/10.1021/ja016238k.
132. C. Yang, C. Ke, W. Liang, et al., *J. Am. Chem. Soc*., **133**, 13786-13789 (2011), https://doi.org/10.1021/ja202020x.
133. M. J. Genzink, J. B. Kidd, W. B. Swords, and T. P. Yoon, *Chem. Rev.,* **122**, 1654-1716 (2022), https://doi.org/10.1021/acs.chemrev.1c00467.
134. M. Alagesan, K. Kanagaraj, S. Wan, et al., *J. Photochem. Photobiol*. A, **331**, 95-101 (2016), https://doi.org/10.1016/j.jphotochem.2015.10.023.
135. R. Li, B. C. Ma, W. Huang, et al., *ACS Catal*., **7**, 3097-3101 (2017), https://doi.org/10.1021/acscatal.7b00490.
136. X. Kang, X. Wu, X. Han, et al., *Chem. Sci*., **11**, 1494-1502 (2020), https://doi.org/10.1039/C9SC04882K.
137. C. Li, Y. Ma, H. Liu, et al., *Chin. J. Catal*., **41**, 1288-1297 (2020), https://doi.org/10.1016/S1872-2067(20)63572-0.
138. P. Wu, C. He, J. Wang, et al., *J. Am. Chem. Soc*., **134**, 14991-14999 (2012), https://doi.org/10.1021/ja305367j.
139. Y. Cui, J. Ai, Y. Duan, et al., *Chem*., **11**, 102390 (2025), https://doi.org/10.1016/j.chempr.2024.102390.
140. P. V. Torchyniuk, O. I. V'yunov, A. A. Ishchenko, et al., *Theor. Exp. Chem*., **60**, 155-176 (2024), https://doi.org/10.1007/s11237-025-09818-y.
141. K. Mishra, D. Guyon, J. San Martin, and Y. Yan, *J. Am. Chem. Soc*., **145**, 17242-17252 (2023), https://doi.org/10.1021/jacs.3c04593.
142. C. Hao, R. Gao, Y. Li, et al., *Angew. Chem. Int. Ed.,* **58**, 7371-7374 (2019), https://doi.org/10.1002/anie.201902673.
143. M. Sun, L. Xu, A. Qu, et al., *Nat. Chem*., **10**, 821-830 (2018), https://doi.org/10.1038/s41557-018-0083-y.
144. H. Zhang, C. Hao, A. Qu, et al., *Angew. Chem. Int. Ed*., **59**, 7131-7138 (2020), https://doi.org/10.1002/anie.202002028.
145. C. Zhang, Y. Li, D. Wang, et al., *Environ. Sci. Pollut. Res*., **22**, 10444-10451 (2015), https://doi.org/10.1007/s11356-015-4251-y.
146. D. Wang, Y. Li, G. Li Puma, et al., *Chem. Commun.,* **49**, 10367-10369 (2013), https://doi.org/10.1039/C3CC45193C.